Supplementary Information (SI) for Energy & Environmental Science.
This journal is © The Royal Society of Chemistry 2024

Electronic Supplementary Information

Resolving molecular diffusion model based on butterfly-shaped non-fused ring electron acceptors for efficient ternary organic photovoltaics with improved stability

Xueyan Ding,‡[a] Xiaoling Wu,‡[a] Shuixing Li,*[b] Tianyi Chen,[a] Jinyang Yu,[a] Heng Liu,[c] Mengting Wang,[a] Xiu-Kun Ye,[a] Nuo Zhang,[a] Xinhui Lu,[c] Chang-Zhi Li,[a] Haiming Zhu,[d] Minmin Shi,[a] Hanying Li[a] and Hongzheng Chen*[ab]

[a] State Key Laboratory of Silicon and Advanced Semiconductor Materials, Department of Polymer Science and Engineering, Zhejiang University, Hangzhou 310058, China. E-mail: hzchen@zju.edu.cn

[b] Zhejiang University-Hangzhou Global Scientific and Technological Innovation Center, Hangzhou 311200, China. E-mail: lishuixing89@zju.edu.cn.

[c] Department of Physics, The Chinese University of Hong Kong, Hong Kong 999077, China.

[d] Department of Chemistry, Zhejiang University, Hangzhou 310058, China.

‡ X. Ding and X. Wu contributed equally to this work.

Supporting Methods

Instruments and Characterizations

^{1}H-NMR and ^{13}C-NMR spectra were obtained on a Bruker Advance III 400 (400 MHz) NMR spectroscope. Matrix-assisted laser desorption ionization time-of-flight (MALDI-TOF) mass spectrum tests were carried out on a Bruker Ultraflextreme MALDI-TOF/TOF mass spectrometry. UV-vis absorption spectra were recorded on a HITACHI U-4100 spectrophotometer. Cyclic voltammetry (CV) measurements were carried out on a CHI600A electrochemical workstation with a standard three-electrode configuration employing a Pt plate as the working electrode, a Pt wire as the counter electrode and a saturated calomel electrode (SCE) as the reference electrode in anhydrous acetonitrile solution containing 0.1 M tetrabutylammonium hexafluorophosphate (Bu_4NPF_6) as the supporting electrolyte. All potentials were calibrated with the standard ferrocene/ferrocenium redox system (Fc/Fc^+) and assumption that the energy level of Fc is 4.8 eV below vacuum. The equation of $E_{LUMO/HOMO}$ = -e($E_{red/ox}$ + 4.41) (eV) was used to calculate the LUMO and HOMO levels (the redox potential of Fc/Fc^+ is found to be 0.39 V). Thermogravimetric analysis (TGA) data were obtained from a WCT-2 thermal balance under N_2 atmosphere at a heating rate of 10 ^{o}C/min. Differential scanning calorimetry (DSC) measurement was performed on a Pekin-Elmer Pyris 1 differential scanning calorimeter under N_2 atmosphere at a scanning rate of 10 °C/min. Contact angle test was conducted on a LAUDA Scientific LSA series video optical contact angle tension measuring instrument. The morphologies of blended films were characterized by a VeecoMultiMode atomic force microscopy (AFM) in the tapping mode. The grazing incident wide-angle X-ray scattering (GIWAXS) measurement was carried out with a Xeuss 2.0 WAXS laboratory beamline using a Cu X-ray source (8.05 keV, 1.54 Å) and a Pilatus3R 300K detector.

DFT Calculation. Density functional theory calculations were conducted at the B3LYP/6-31G(d) level to obtain the optimized molecular geometries and the surface electrostatic potential (ESP) distribution. The long alkyl side-chains were replaced by methyl groups to save time.

Device Fabrication. Organic solar cells were fabricated with the conventional structure of ITO/PEDOT:PSS/Active layer/PDINN/Ag. Before fabrication, the ITO coated glass substrates were cleaned by ultrasonic treatment in detergent, deionized water, acetone, isopropyl alcohol and alcohol under ultrasonication for 10 min in each step. And then the ITO substrates were treated in the ultraviolet cleaner (UC100-SE, LEBO Science) for 10 min before being spin-coated at 4500 rpm with a layer of 10 nm thickness PEDOT:PSS (Clevios^{TM} 4083). After baking the PEDOT:PSS layer in air at 150 ℃ for 10 min, the substrates were transferred to the N_2 glovebox. The active layer materials D18:X7-D (1:1.4 *w*/*w*), D18:X8-D (1:1.4 *w*/*w*), D18:Y6 (1:1.6 *w*/*w*), D18:Y6:X7-D (1:1.4:0.2 *w*/*w*), D18:Y6:X8-D (1:1.5:0.2 *w*/*w*) were dissolved in chloroform at a polymer concentration of 4.5 mg/ml. All the active layer solutions were heated and stirred at 95 ℃ for 1 hour before spin coating. Before spin coating the active layer, 3,5-dichlorobromobenzene (DCBB) was first dissolved in chloroform 10 mg/ml for 10 min, and then active layer materials were dissolved in the DCBB solutions. Then, the DCBB-processed active layer films were annealed at 90°C for 10 min. A thin layer of PDINN was spin-coated from 1.5 mg mL^{-1} methanol solution on the top of the active layer. Finally, the Ag (100 nm) electrode was deposited by thermal evaporation to complete the device with an active area of 6 mm^2, and the testing aperture area is 4.572 mm^2.

***J-V* and EQE Measurement.** The *J-V* measurement was performed via the solar simulator (SS-X50, Enlitech) and AM 1.5G spectra, calibrating the intensity of the certified standard silicon solar cell (KG2) at 100 mW cm^{-2}. The external quantum efficiency (EQE) data were obtained using the solar-cell spectral-response measurement system (RE-R, Enlitech).

Space Charge Limited Current (SCLC) Measurement. The hole and electron mobilities of binary or ternary films in OSCs were measured using space charge limited current (SCLC) measurements. Hole-only devices were fabricated in a structure of ITO/PEDOT:PSS/Active layer/MoO_3/Ag, and electron-only devices were fabricated in a structure of ITO/ZnO/Active layer/PDINN/Ag. The device characteristics were extracted by modeling the dark current under forward bias using the SCLC expression described by the Mott-Gurney law:[1]

$$J = \frac{9}{8}\varepsilon_r\varepsilon_0\mu\frac{V^2}{L^3}$$

where J is the current density, $\varepsilon_r \approx 3$ is the average dielectric constant of the blended film, ε_0 is the permittivity of the free space, μ is the carrier mobility, L is the thickness of the film (~100 nm), and V is the applied voltage.

Transient Absorption Spectroscopy (TAS) Measurement. For femtosecond transient absorption spectroscopy, the fundamental output from Yb:KGW laser (1030 nm, 220 fs Gaussian fit, 100 kHz, Light Conversion Ltd) was separated to two light beams. One was introduced to NOPA (ORPHEUS-N, Light Conversion Ltd) to produce a certain wavelength for pump beam (here we use 750 nm, <10 μJ/cm^2), the other was focused onto a YAG plate to generate white light continuum as probe beam. The pump and probe overlapped on the sample at a small angle less than 10°. The transmitted probe light from sample was collected by a linear CCD array. Then we obtained transient differential transmission signals by equation shown below:

$$\frac{\Delta T}{T} = \frac{T_{pump-on} - T_{pump-off}}{T_{pump-off}}$$

We processed the analysis of hole transfer kinetics by biexponential fitting based on the following formula:

$$i = A_1 e^{-t/\tau_1} + A_2 e^{-t/\tau_2}$$

Estimation of Glass-Transition Temperature. Following the method reported by Harald Ade,[2] the thermal transition was studied by observing shifts in the UV-vis absorption spectrum after thermal annealing of various pristine film samples. Then, a deviation metric (DM_T) was calculated by quantifying the change in the absorbance of each film during annealing by the following formula:

$$DM_T = \sum_{\lambda_{min}}^{\lambda_{max}} [I_{RT}(\lambda) - I_T(\lambda)]^2$$

where λ is the wavelength, and λ_{min} and λ_{max} are the lower and upper bounds of the optical sweep, $I_{RT}(\lambda)$ and $I_T(\lambda)$ are the normalized absorption intensities of the as-cast (room temperature) and annealed films, respectively.

Time-of-Flight Secondary Ion Mass Spectrometry (TOF-SIMS) Measurements.

Preparation of donor:acceptor bilayer films: Acceptors Y6, X7-D, X8-D, Y6:X7-D (7:1 *w*/*w*), Y6:X8-D (7:1 *w*/*w*), and polymer donor D18 were separately dissolved in chloroform (CF) overnight. The concentrations of the acceptors and donor were 35 mg/mL and 7 mg/mL respectively. The dissolved acceptors and neat donor solution were spin-coated onto an Indium Tin Oxide (ITO) substrate and polystyrene sulfonate (PSS)-coated glass, respectively, at 800 rpm. Afterward, both donor and acceptor films were vacuum dried at room temperature for one day to remove the residual amount of processing solvent before making the bilayer sample. The donor films were carefully floated on deionized (DI) water and then picked up with the ITO-supported acceptor films, creating a bilayer structure on the ITO substrates. The formed bilayer films were kept at room temperature overnight and were subsequently moved to a vacuum chamber at room temperature and were kept for 12 hours to remove the residual amount of water trapped at the interface between donor and acceptor.

TOF-SIMS Measurement Conditions: Dual-beam dynamic SIMS mode was used to provide high depth resolution and chemical resolution simultaneously, where Bi^{3+} was used as the primary ion and Cs^{+} was used as the sputtering source. The sputtering ions with an energy of 0.5 keV and the sputter ares was 200 μm by 200 μm. Notably, the CN^{-} signal is utilized to effectively track the distribution of acceptors.

Diffusion coefficient extraction.

To account for the polymer donor layer being on top of the acceptors layer, we obtained the fitted diffusion profile of the acceptors into the donor using the error function (erfc) from Fick's 2nd law, as shown below:

$$C(t, t_a) = C_0 erfc\left(\frac{-r_s(t - t_0)}{2\sqrt{Dt_a}}\right)$$

Where $C(t,t_a)$ represents the concentration as a function of annealing time t_a and sputtering time t. C_0 represents the concentration near the interface between the polymer donor and small molecule acceptor, which corresponds to the constant concentration of the acceptor source. D is the diffusion coefficient, t_0 is sputter time that defines the interface location (close to 50 vol% NF-SMA), and r_s is the sputtering rate, determined by the ratio of the film thickness to sputtering time.

Time-resolved UV-vis

The in-situ UV-vis spectra were measured using a spectrometer (ATP SERIES). The light source was a halogen lamp. The spin-coating process is controlled as the same for the device fabrication.

Materials and synthesis

Materials. Non-fullerene acceptors of X7-D and X8-D were synthesized according to the following procedures. Polymer donor of D18 and non-fullerene acceptor of Y6 were purchased from Solarmer Energy Inc. PDINN was purchased from Organtec Ltd. PEDOT:PSS (P Al 4083) was purchased from Heraeus Clevios^{TM}. Other chemical reagents and solvents were purchased from commercial suppliers and used without further purification.

Synthesis.

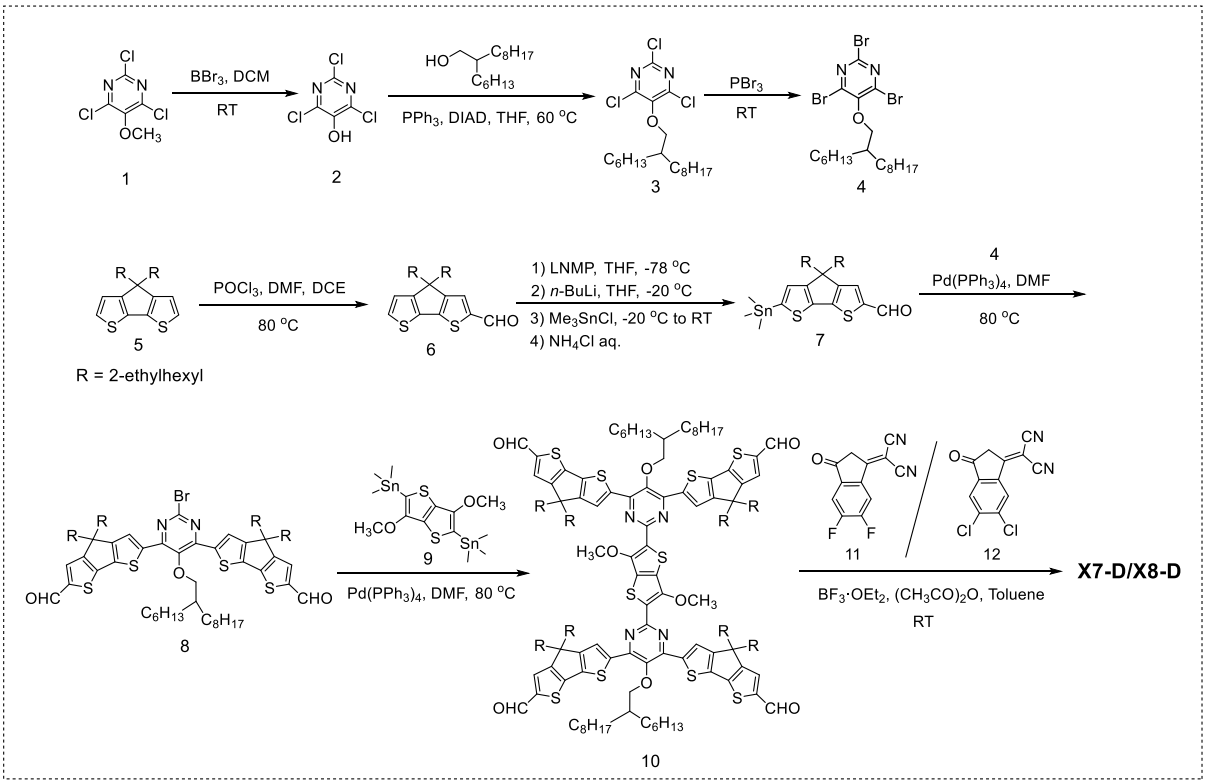

Scheme S1 Synthetic routes of X7-D and X8-D.

Synthesis of Compound 2

To a round-bottom flask were added **Compound 1** (2.50 g, 11.7 mmol) and dichloromethane (80 ml). Then, 1 M solution of boron tribromide in dichloromethane (41 mL, 41.0 mmol) was added dropwise at 0 ^{o}C, and the resulting mixture was stirred at room temperature for 16 h. After cooling to 0 ^{o}C, the reaction mixture was diluted by the sequential addition of methanol and water. Then, the crude product was extracted with dichloromethane, and dried with anhydrous Na_2SO_4. After removing the solvent, the product was dried under vacuum, yielding an off-white solid (2.31 g, 11.6 mmol, 99% yield). This product was used directly in the next step without further purification.

Synthesis of Compound 3

To a two-necked round-bottom flask were added **Compound 2** (2.00 g, 10.0 mmol), 2-hexyldecan-1-ol (3.65 g, 15.0 mmol), PPh_3 (3.93 g, 15.0 mmol) and THF (60 mL). The mixture was frozen by liquid nitrogen, followed by three times of successive vacuum and argon fill cycles. Under the protection of argon, DIAD (2.95 mL, 15.0 mmol) was injected. Then, the reactant was refluxed at 60 ^{o}C for 20 h. After pouring into water, the crude product was extracted with dichloromethane, and dried with anhydrous $MgSO_4$. After removing the solvent, silica gel column chromatography was used to purify the product with the mixture of petroleum ether and ethyl acetate (1:0 ~ 20:1) as the eluent, yielding a colorless oil (3.75 g, 88%). ^{1}H NMR (400 MHz, $CDCl_3$, ppm): δ = 3.97 (d, J = 5.2 Hz, 2H), 1.84-1.76 (m, 1H), 1.57-1.46 (m, 2H), 1.36-1.17 (m, 20H), 0.91-0.83 (m, 6H).

Synthesis of Compound 4

To a two-necked round-bottom flask were added **Compound 3** (3.75 g, 8.85 mmol) and PBr_3 (20 mL). The mixture was frozen by liquid nitrogen, followed by three times of successive vacuum and argon fill cycles. Then, the reactant was refluxed at 80 ^{o}C for 20 h. After removing the remaining PBr_3, silica gel column chromatography was used to purify the product with the mixture of petroleum ether and ethyl acetate (1:0 ~ 20:1) as the eluent, yielding a colorless oil

4.00 g, 81%). ^{1}H NMR (400 MHz, $CDCl_3$, ppm): δ = 3.97 (d, *J* = 5.6 Hz, 2H), 1.90-1.80 (m, 1H), 1.60-1.49 (m, 2H), 1.36-1.21 (m, 20H), 0.93-0.85 (m, 6H).

Synthesis of Compound 6

Under the protection of argon, 5 mL of DMF was added to a two-necked round-bottom flask. Then, $POCl_3$ (1.5 mL, 14.7 mmol) was injected at 0 °C. After being stirring at 0 °C for 0.5 h, **Compound 4** (5.0 g, 12.4 mmol) dissolved in 30 mL DCE was injected. Then, the mixture was refluxed at 80 °C for 8 h. After cooling, $NaHCO_3$ aqueous solution was added, and the mixture was stirred overnight. The crude product was extracted with dichloromethane, washed with water, and dried with anhydrous $MgSO_4$. After removing the solvent, silica gel column chromatography was used to purify the product with the mixture of petroleum ether and dichloromethane (1:1) as the eluent, yielding a deep-yellow oil (4.28 g, 80%). ^{1}H NMR (400 MHz, $CDCl_3$, ppm): δ = 9.83 (s, 1H), 7.57 (t, *J* = 3.6 Hz, 1H), 7.38 (d, *J* = 4.9 Hz, 1H), 7.00 (dt, *J* = 4.9, 2.4 Hz, 1H), 1.99-1.85 (m, 4H), 1.03-0.83 (m, 16H), 0.74 (t, *J* = 6.8 Hz, 6H), 0.63-0.54 (m, 8H).

Synthesis of Compound 7

To a two-necked round-bottom flask were added **Compound 6** (4.00 g, 9.3 mmol) and THF (40 mL). The mixture was frozen by liquid nitrogen, followed by three times of successive vacuum and argon fill cycles. After cooling to -78 °C, 1 mL *N*-methyl piperazine (NMP) was injected. Then, *n*-BuLi (6.2 mL, 9.9 mmol, 1.6 M) was added dropwise, and the mixture was stirred for 0.5 h at -78 °C. After warming to -20 °C, another portion of *n*-BuLi (6.2 mL, 9.9 mmol, 1.6 M) was added dropwise, and the reactant was stirred for 0.5 h. Then, at -20 °C, Me_3SnCl (9.6 mL, 9.6 mmol, 1 M) was injected. After warming to room temperature, the mixture was stirred overnight. Then, the crude product was poured into water, extracted with dichloromethane, and dried with anhydrous $MgSO_4$. After removing the solvent, the product was dried under vacuum, yielding a deep red oil (4.13 g, 75%). ^{1}H NMR (400 MHz, $CDCl_3$, ppm): δ = 9.81 (s, 1H), 7.55 (t, *J* = 4.5 Hz, 1H), 7.02 (t, *J* = 3.1 Hz, 1H), 1.96-1.88 (m, 4H), 1.06-0.85 (m, 16H), 0.79-0.71 (m, 6H), 0.62-0.54 (m, 8H), 0.39 (s, 9H).

Synthesis of Compound 8

To a two-necked round-bottom flask were added **Compound 4** (1.00 g, 1.80 mmol), **Compound 7** (2.67 g, 4.49 mmol), $Pd(PPh_3)_4$ (0.311 g, 0.270 mmol) and DMF (30 mL). The mixture was frozen by liquid nitrogen, followed by three times of successive vacuum and argon fill cycles. Then, the reactant was refluxed at 80 °C for 48 h. After pouring into water, the crude product was extracted with dichloromethane, and dried with anhydrous $MgSO_4$. After removing the solvent, silica gel column chromatography was used to purify the product with the mixture of petroleum ether and dichloromethane (1:1 ~ 1:2) as the eluent, yielding an orange solid (1.70 g, 75%). ^{1}H NMR (400 MHz, $CDCl_3$, ppm): δ = 9.88 (s, 2H), 8.11 (t, *J* = 8.6 Hz, 2H), 7.63 (t, *J* = 3.5 Hz, 2H), 3.83 (d, *J* = 7.4 Hz, 2H), 2.31-2.19 (m, 1H), 2.08-1.87 (m, 8H), 1.65-1.40 (m, 4H), 1.38-1.16 (m, 24H), 1.08-0.80 (m, 32H), 0.77-0.54 (m, 30H). ^{13}C NMR (400 MHz, $CDCl_3$, ppm): δ = 182.72, 162.33, 159.41, 155.22, 154.29, 146.59, 145.09, 143.49, 142.19, 141.25, 130.54, 126.46, 54.28, 54.25, 54.23, 43.44, 43.25, 39.38, 35.37, 35.33, 34.24 , 34.21, 33.88, 31.91, 31.80, 31.41, 30.28, 29.91, 29.64, 29.41, 28.51, 28.42, 27.52, 27.22, 27.18, 27.04, 27.00, 22.79, 22.70, 14.15, 14.13, 14.09, 14.04, 10.68, 10.59.

Synthesis of Compound 10

To a two-necked round-bottom flask were added **Compound 8** (1.50 g, 1.19 mmol), **Compound 9** (0.209 g, 0.397 mmol), $Pd(PPh_3)_4$ (0.023 g, 0.020 mmol) and DMF (30 mL). The mixture was frozen by liquid nitrogen, followed by three times of successive vacuum and argon fill cycles. Then, the reactant was refluxed at 80 °C for 48 h. After pouring into water, the crude product was extracted with dichloromethane, and dried with anhydrous $MgSO_4$. After removing the solvent, silica gel column chromatography was used to purify the product with the mixture of petroleum ether and dichloromethane (1:1 ~ 1:3) as the eluent, yielding an orange solid (0.628 g, 62%). ^{1}H NMR (400 MHz, $CDCl_3$, ppm): δ = 9.91 (s, 2H), 8.16 (t, *J* = 7.6 Hz, 2H), 7.65 (t, *J* = 3.5 Hz, 2H), 4.47 (s, 3H), 3.90 (d, *J* = 7.4 Hz, 2H), 2.28-2.18 (m, 1H), 2.13-1.92 (m, 8H), 1.71-1.45 (m, 4H), 1.44-1.20 (m, 24H), 1.11-0.85 (m, 32H), 0.81-0.60 (m, 30H). ^{13}C NMR (400 MHz, $CDCl_3$, ppm): δ = 182.81, 182.74, 182.67, 162.87, 162.80, 162.72, 158.99, 155.72, 152.73, 151.51, 147.27, 144.62, 144.17, 142.23, 140.99, 131.82, 130.54, 125.85, 61.02, 54.25, 54.21, 54.17, 43.56, 43.46, 39.72, 35.41, 35.35, 34.33, 33.94, 31.93, 31.86, 31.63, 30.39, 30.02,

29.73, 29.66, 29.43, 28.60, 28.44, 27.55, 27.25, 27.20, 27.14, 22.81, 22.73, 22.71, 14.15, 14.13, 14.10, 14.05, 10.73, 10.71, 10.59, 10.56.

Synthesis of Compound X7-D and X8-D

X7-D and X8-D was prepared by the method from the literature report.[3] To a round-bottom flask were added **Compound 10** (0.300 mg, 0.118 mmol), **Compound 11** (0.054 g, 0.236 mmol) or **Compound 12** (0.062 g, 0.236 mmol) and dry toluene (10 mL). Subsequently, $BF_3{\cdot}OEt_2$ (0.2 mL) and acetic anhydride (0.4 ml) was injected to the above solution and the mixture was stirring at room temperature for 2 h. Then, the reaction mixture was dropwise into methanol, and the precipitate was collected as a crude product. The crude product was purified using silica gel column chromatography with the mixture of petroleum ether and dichloromethane (1:1 ~ 1:4) as the eluent. **X7-D**: brown solid (0.380 g, 95%). ^{1}H NMR (400 MHz, $CDCl_3$, ppm) δ = 8.97 (s, 2H), 8.57 (dd, *J* = 9.9, 6.4 Hz, 2H), 8.21 (t, *J* = 7.4 Hz, 2H), 7.77-7.69 (m, 4H), 4.56 (s, 3H), 3.93 (d, *J* = 7.4 Hz, 2H), 2.30-2.21 (m, 1H), 2.16-1.97 (m, 8H), 1.72-1.62 (m, 2H), 1.53-1.23 (m, 24H), 1.10-0.94 (m, 28H), 0.93-0.85 (m, 6H), 0.84-0.63 (m, 30H). MS (MALDI-TOF) *m/z*: calcd for $C_{200}H_{228}F_8N_{12}O_8S_{10}$ 3400.687; found, 3400.853. **X8-D**: brown solid (0.383 g, 92%) ^{1}H NMR (400 MHz, $CDCl_3$, ppm) δ = 9.00 (s, 2H), 8.80 (s, 2H), 8.21 (t, *J* = 7.2, Hz, 2H), 7.98 (s, 2H), 7.78-7.71 (m, 2H), 4.57 (s, 3H), 3.93 (d, *J* = 7.4 Hz, 2H), 2.30-2.21 (m, 1H), 2.16-1.97 (m, 8H), 1.72-1.62 (m, 2H), 1.53-1.24 (m, 24H), 1.10-0.94 (m, 28H), 0.93-0.85 (m, 6H), 0.84-0.63 (m, 30H). MS (MALDI-TOF) *m/z*: calcd for $C_{200}H_{228}Cl_8N_{12}O_8S_{10}$ 3532.300; found, 3532.955.

Supporting figures

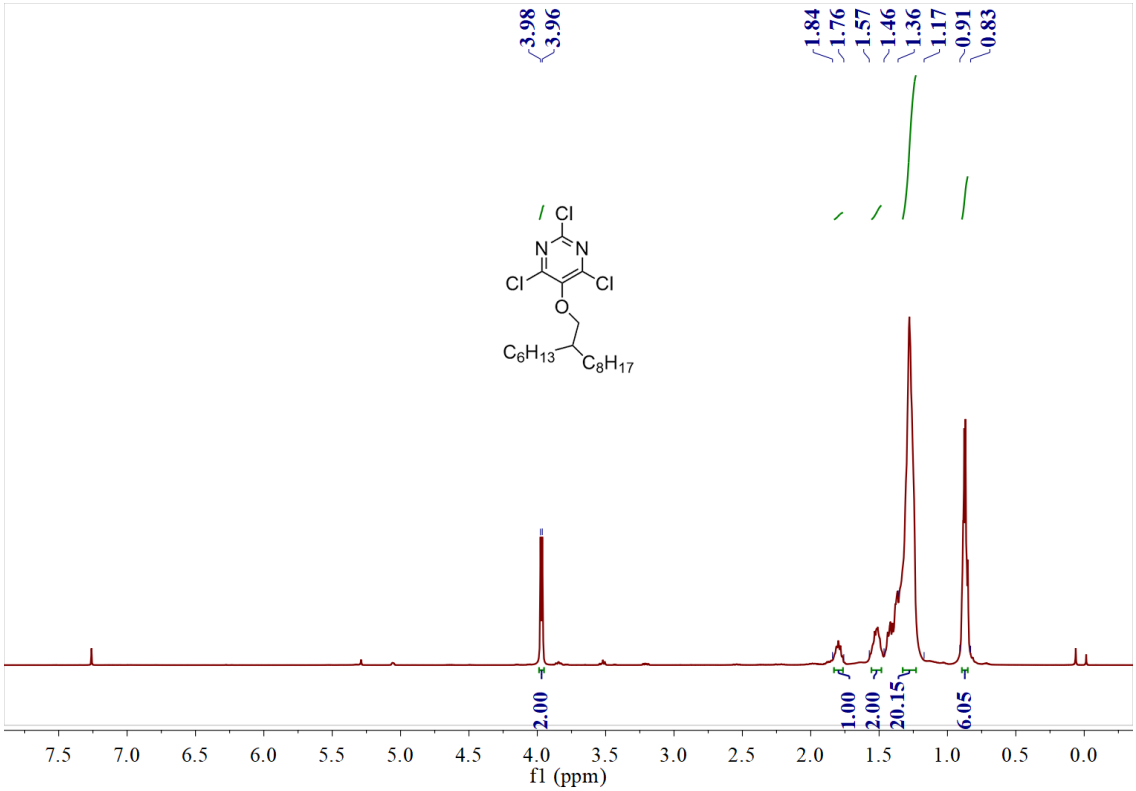

Fig. S1 ^{1}H NMR spectrum of **Compound 3** in $CDCl_3$.

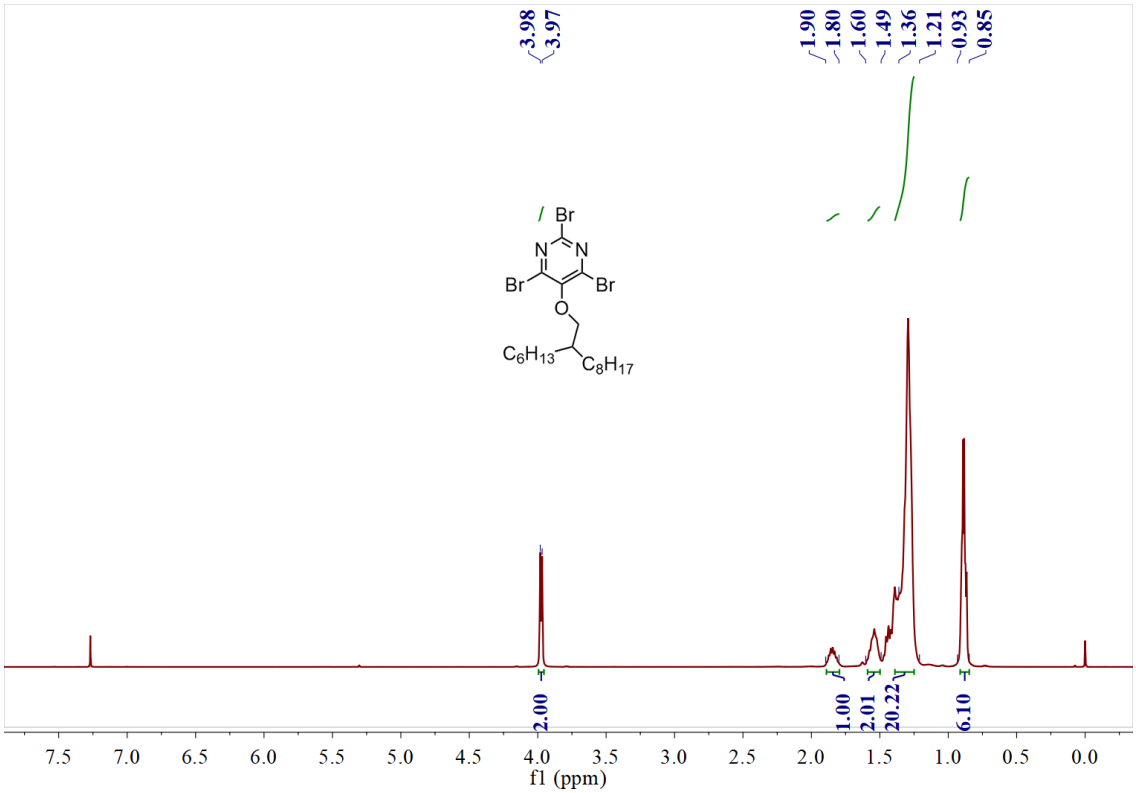

Fig. S2 ^{1}H NMR spectrum of **Compound 4** in $CDCl_3$.

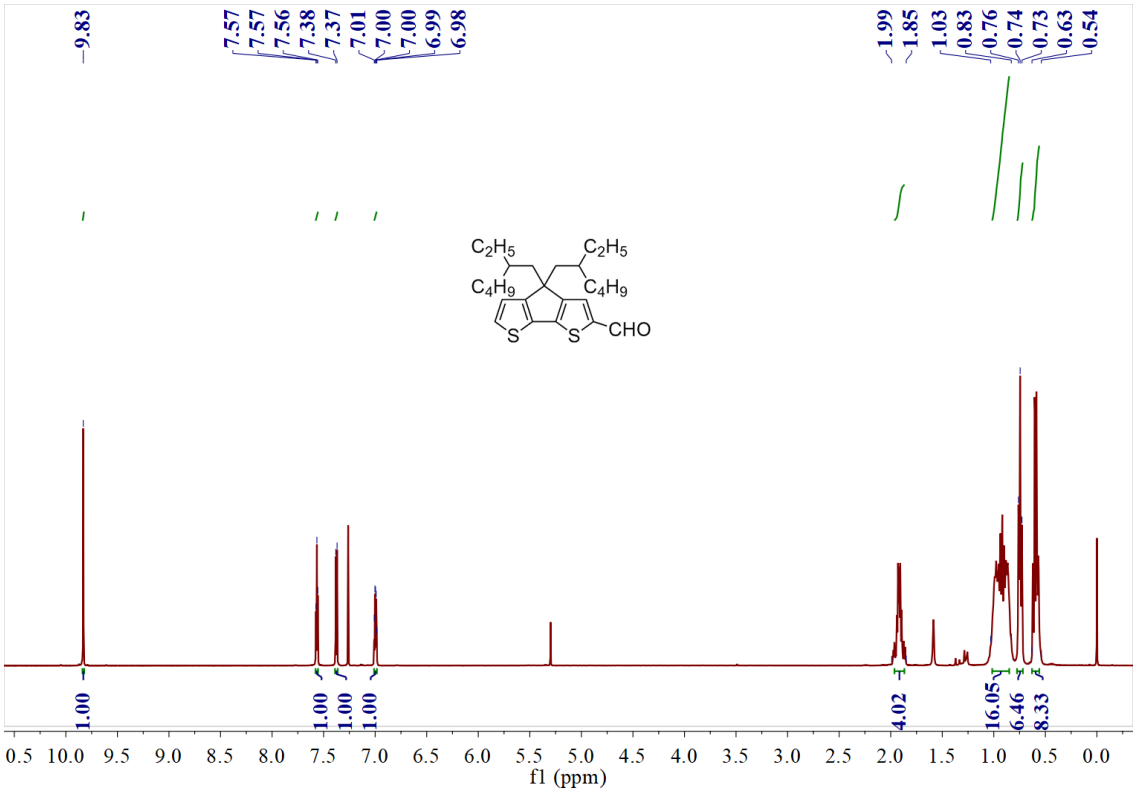

Fig. S3 ^{1}H NMR spectrum of **Compound 6** in $CDCl_3$.

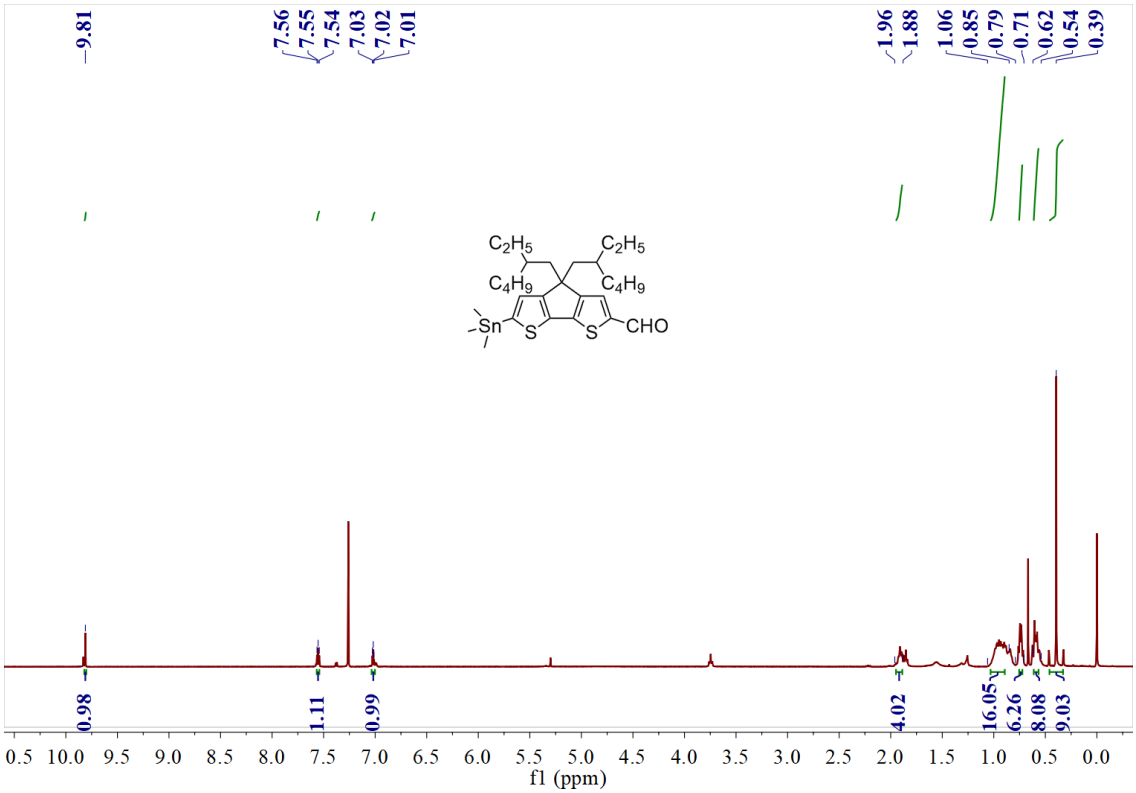

Fig. S4 ^{1}H NMR spectrum of **Compound 7** in $CDCl_3$.

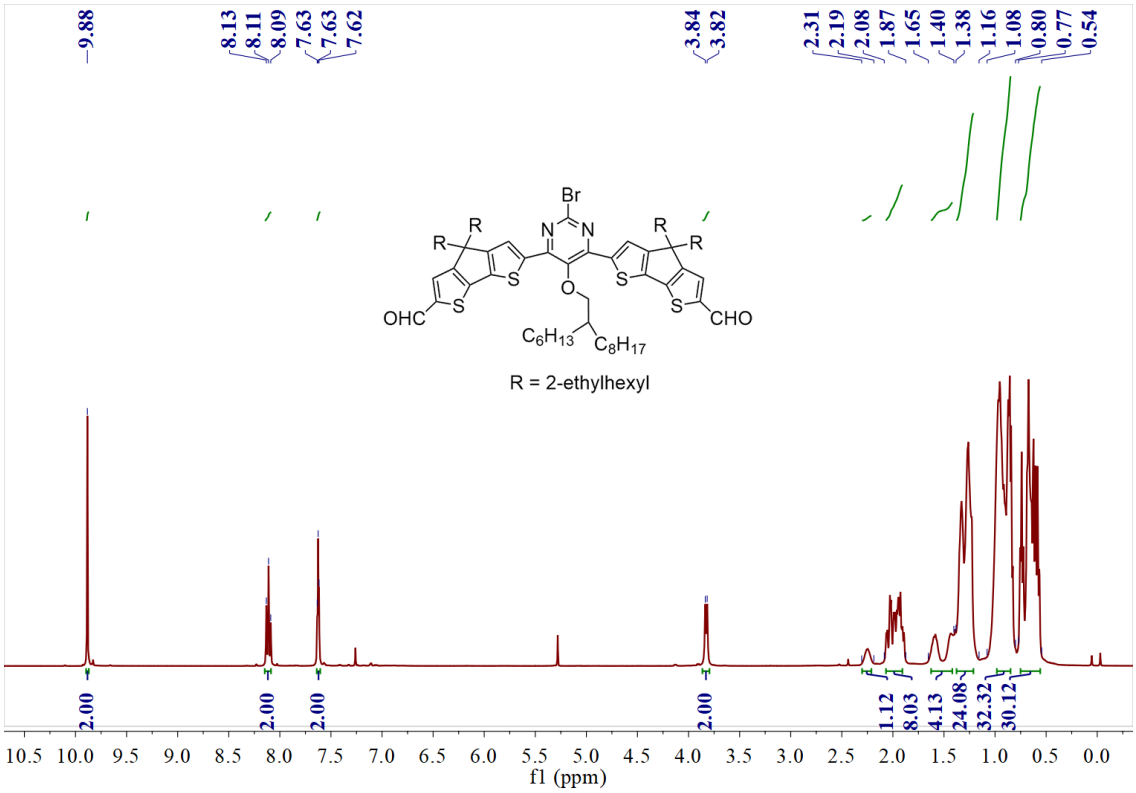

Fig. S5 ^{1}H NMR spectrum of **Compound 8** in $CDCl_3$.

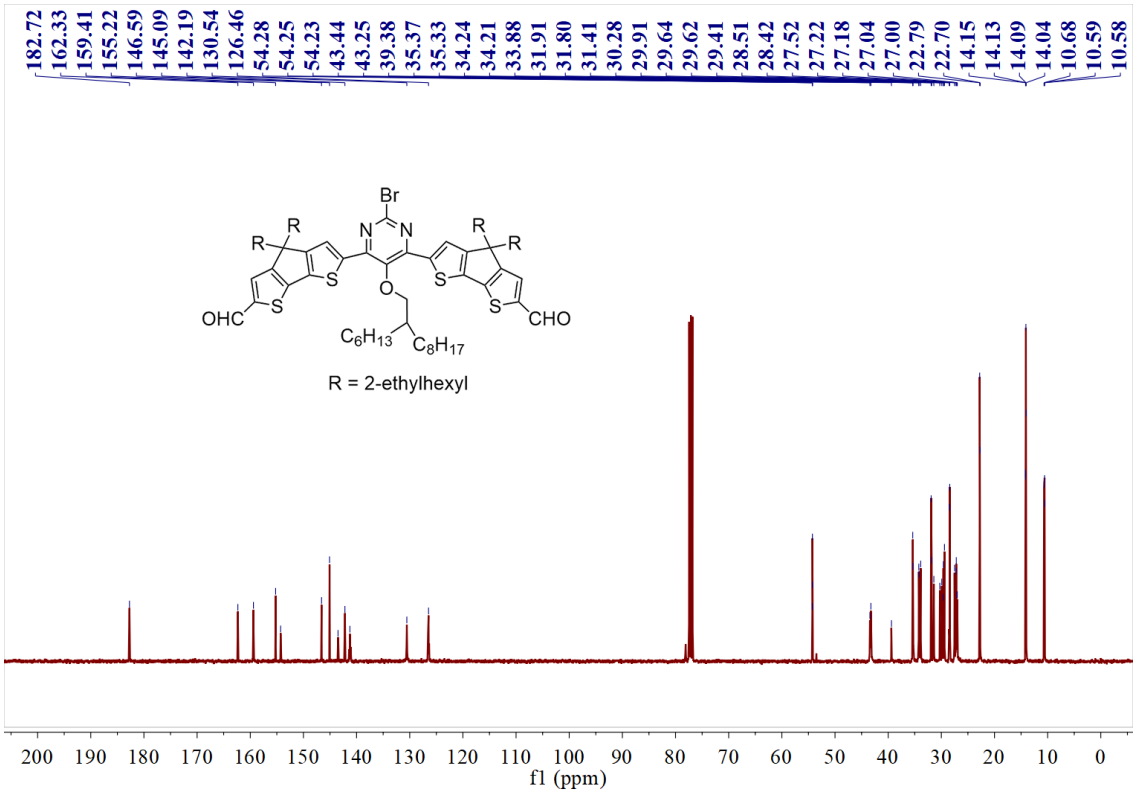

Fig. S6 ^{13}C NMR spectrum of **Compound 8** in $CDCl_3$.

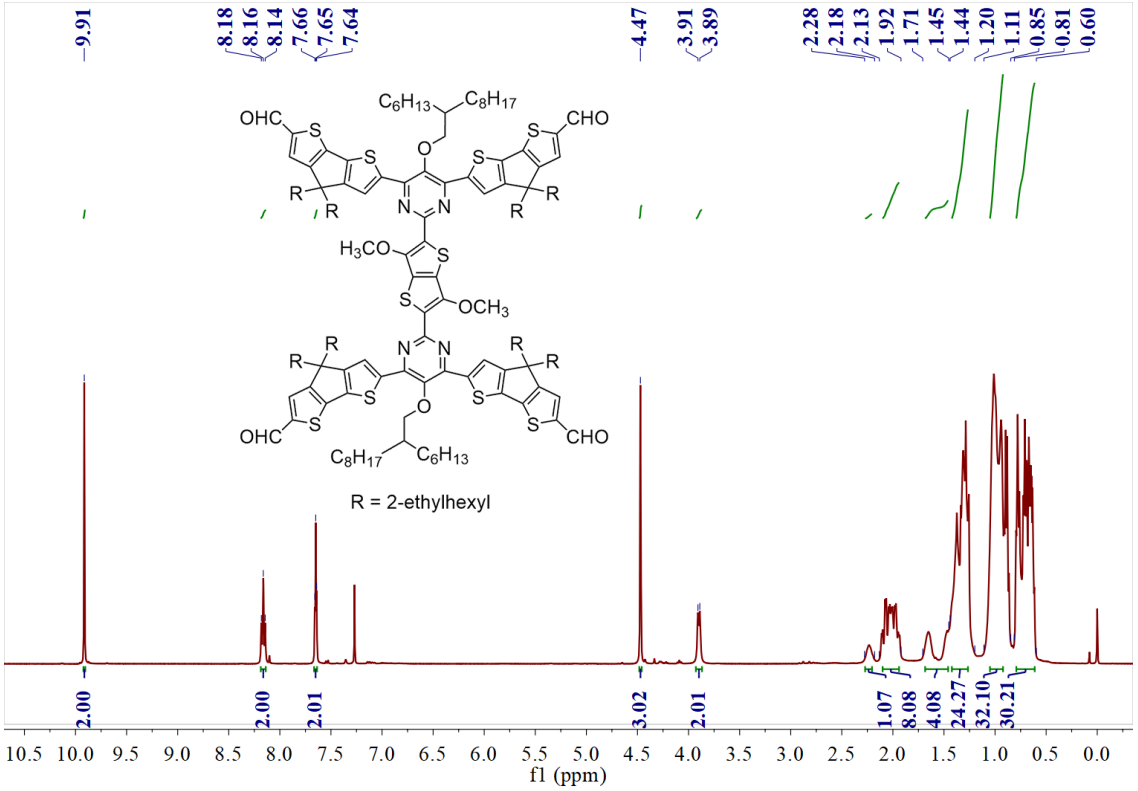

Fig. S7 ^{1}H NMR spectrum of **Compound 10** in $CDCl_3$.

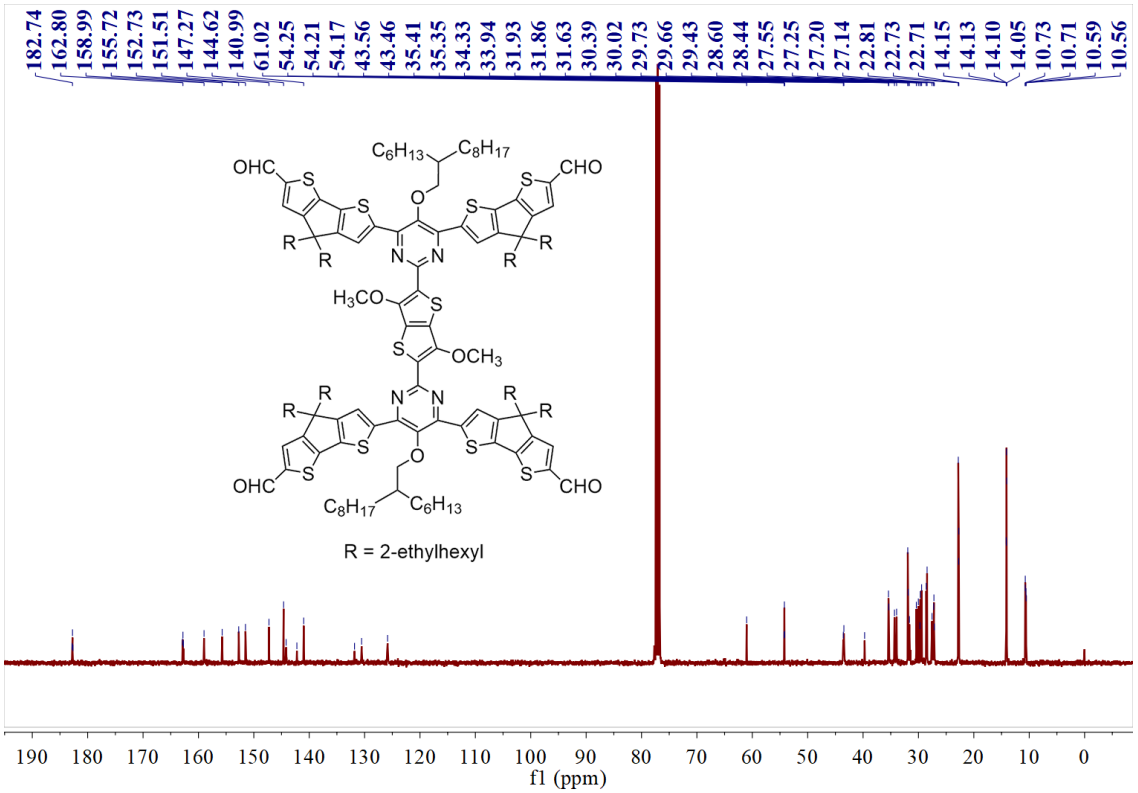

Fig. S8 ^{13}C NMR spectrum of **Compound 10** in $CDCl_3$.

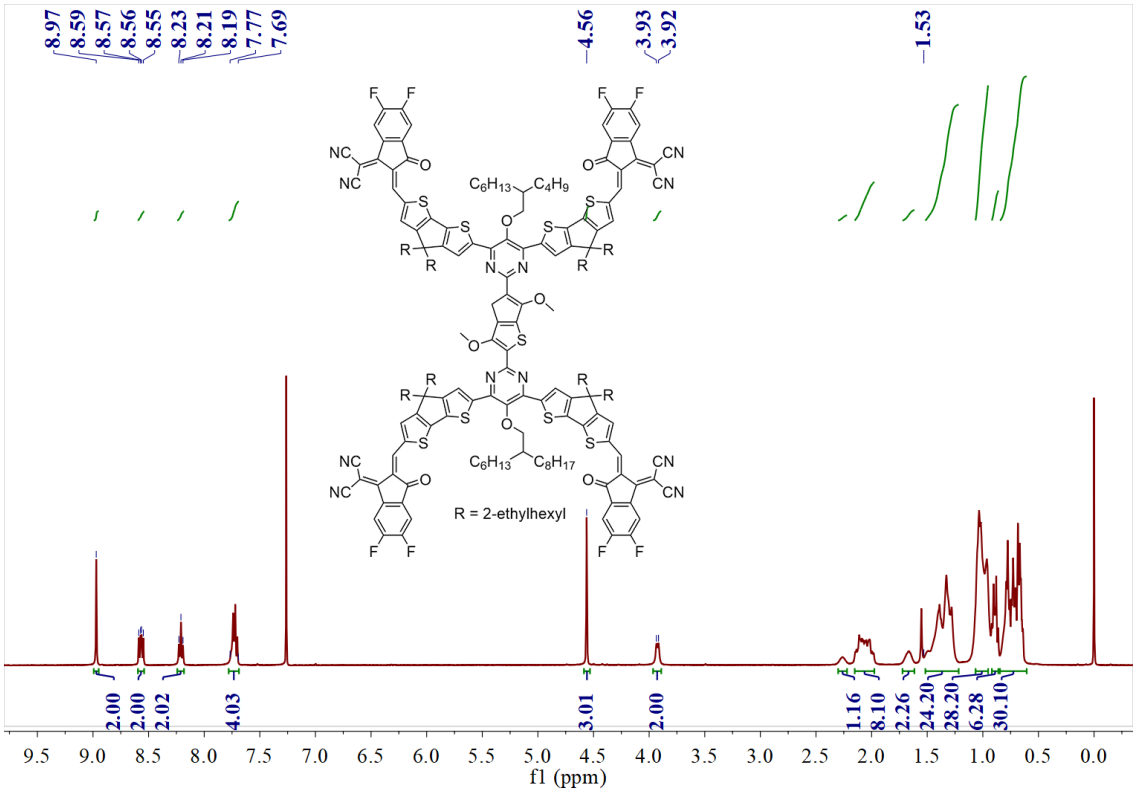

Fig. S9 ^{1}H NMR spectrum of **X7-D** in $CDCl_3$.

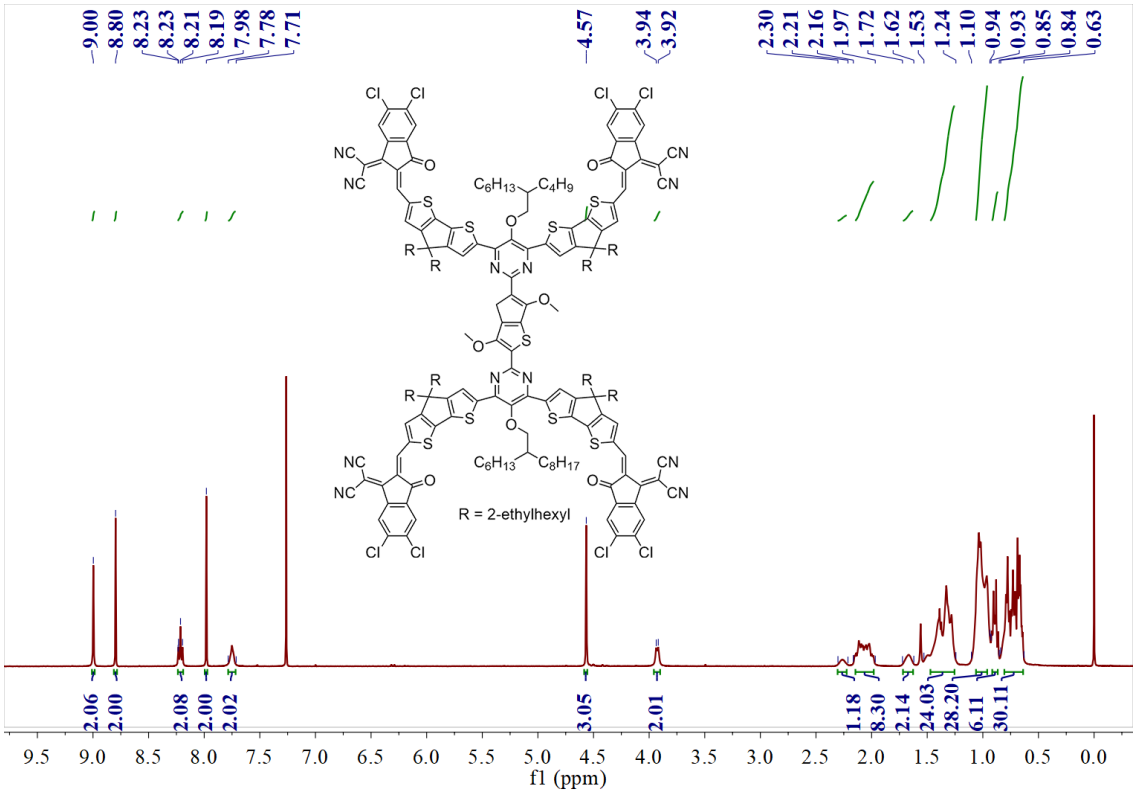

Fig. S10 ^{1}H NMR spectrum of **X8-D** in $CDCl_3$.

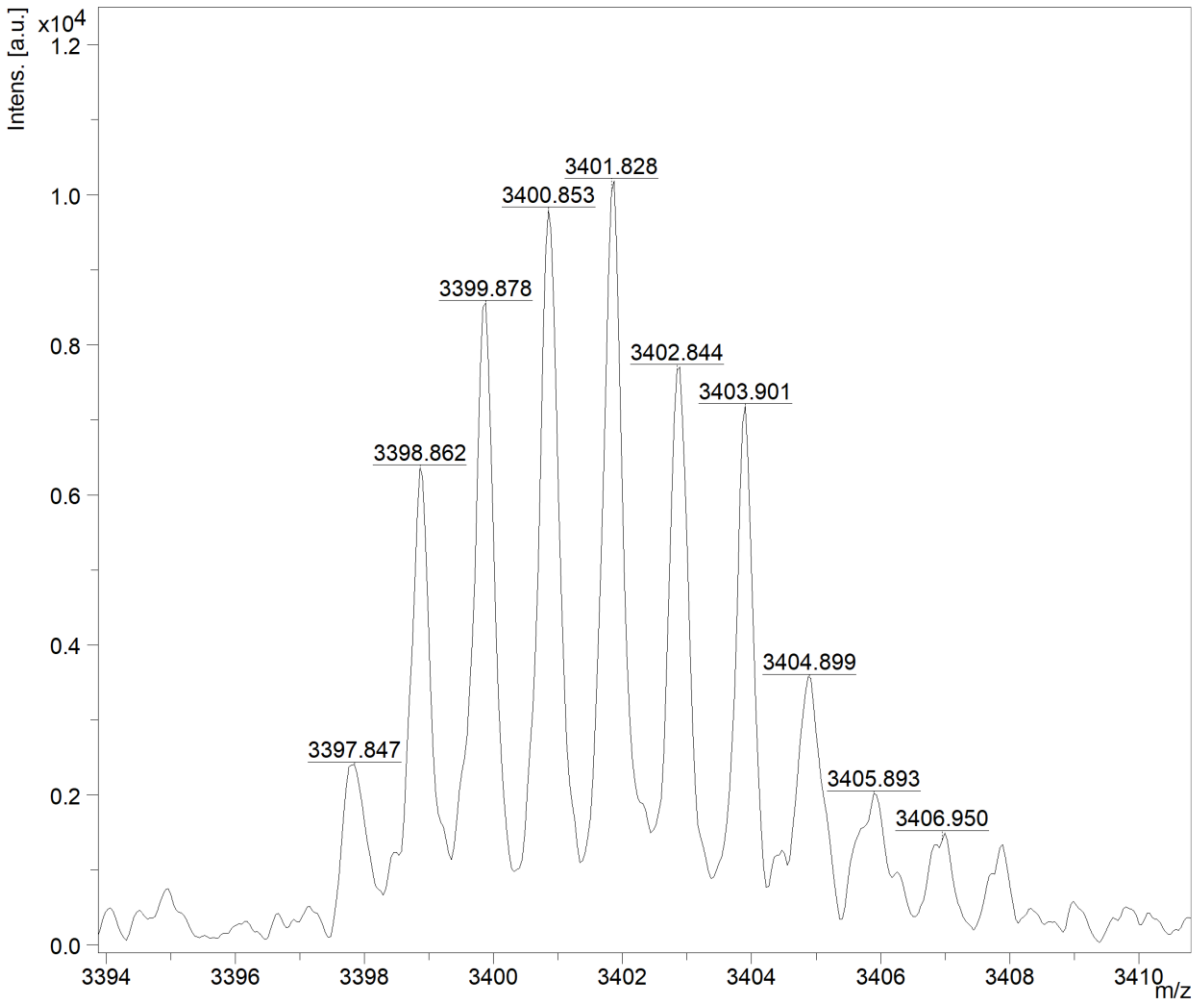

Fig. S11 MALDI-TOF mass spectrum of **X7-D**.

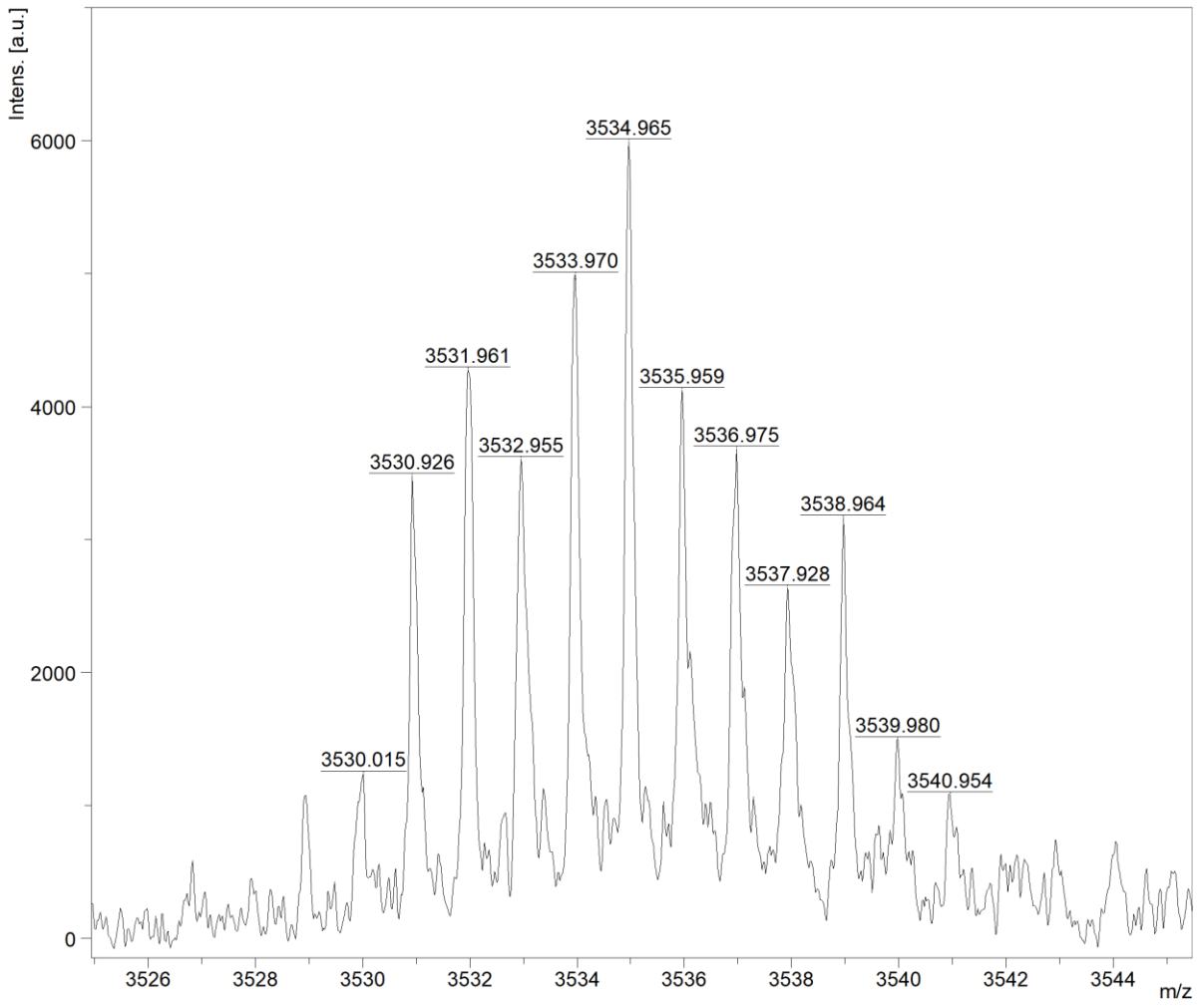

Fig. S12 MALDI-TOF mass spectrum of **X8-D**.

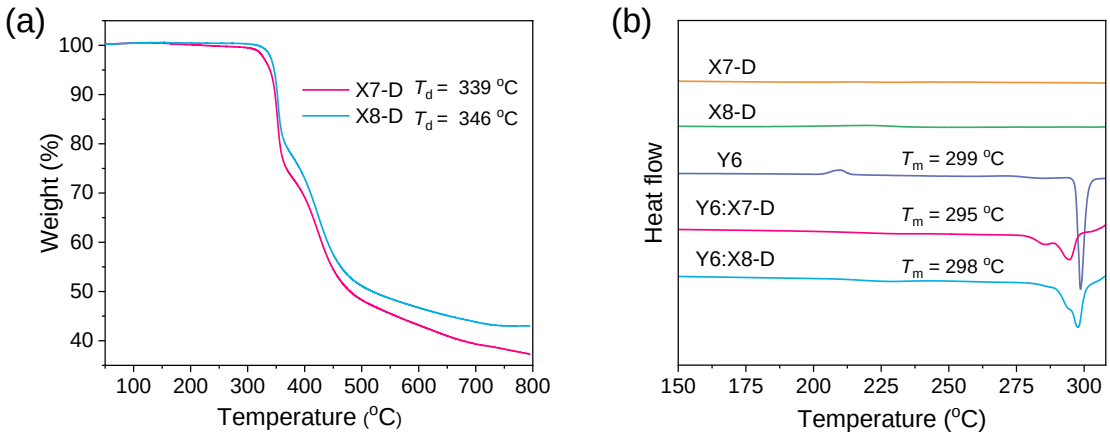

Fig. S13 (a) TGA curves of X7-D and X8-D. (b) DSC heating curves of X7-D, X8-D, Y6, Y6:X7-D (7:1), and Y6:X8-D (7:1) mixtures.

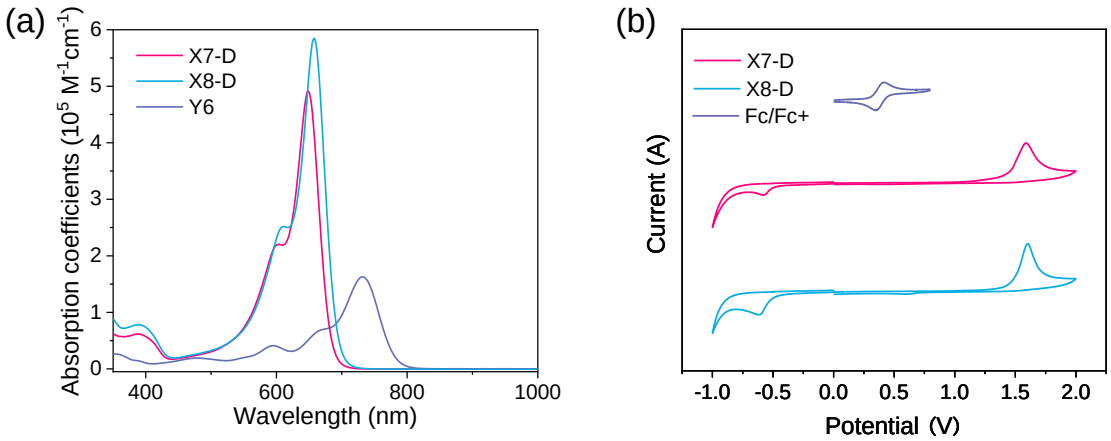

Fig. S14 (a) The absorption coefficients of X7-D, X8-D and Y6 in chloroform. (b) Cyclic voltammetry curves of X7-D, X8-D and ferrocene.

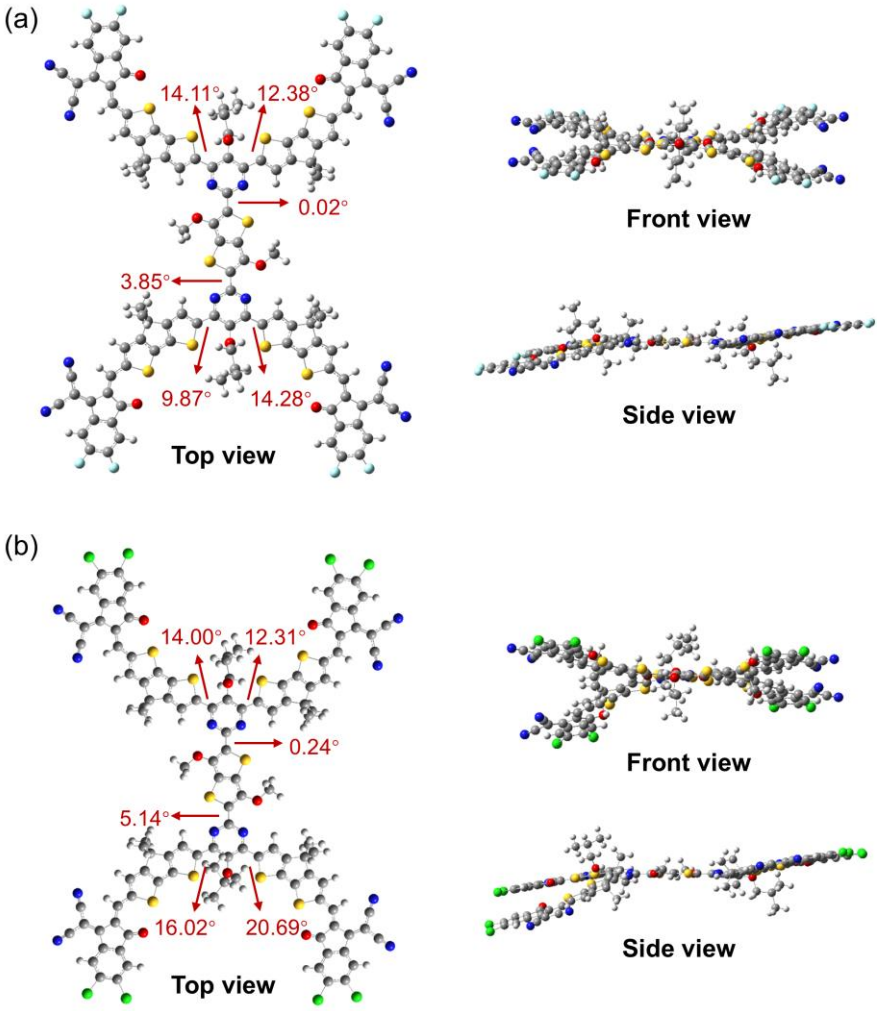

Fig. S15 Optimized molecular configuration of (a) X7-D and (b) X8-D.

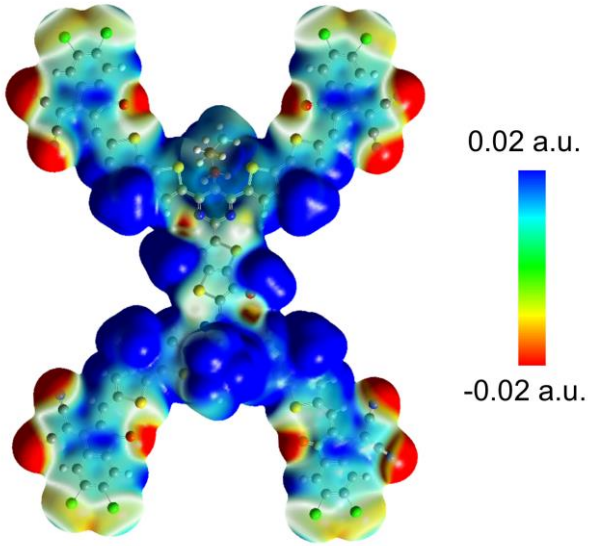

Fig. S16 The surface electrostatic potential distributions for X8-D.

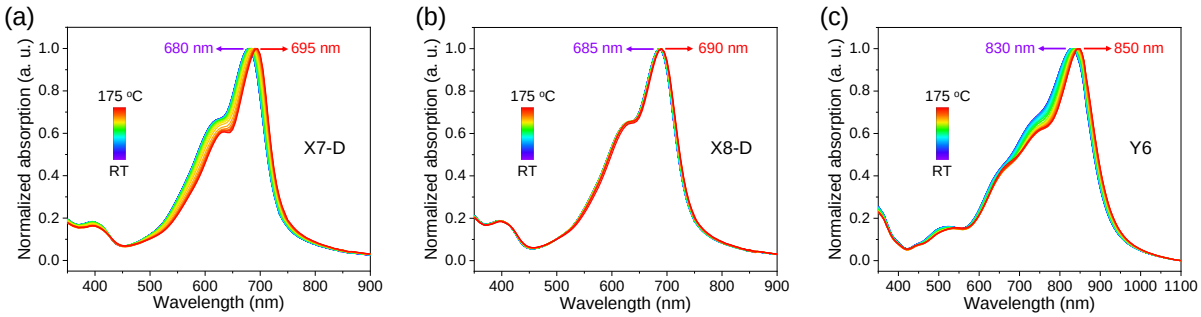

Fig. S17 The temperature-dependent absorption spectra of (a) X7-D, (b) X8-D, and (c) Y6 pure films.

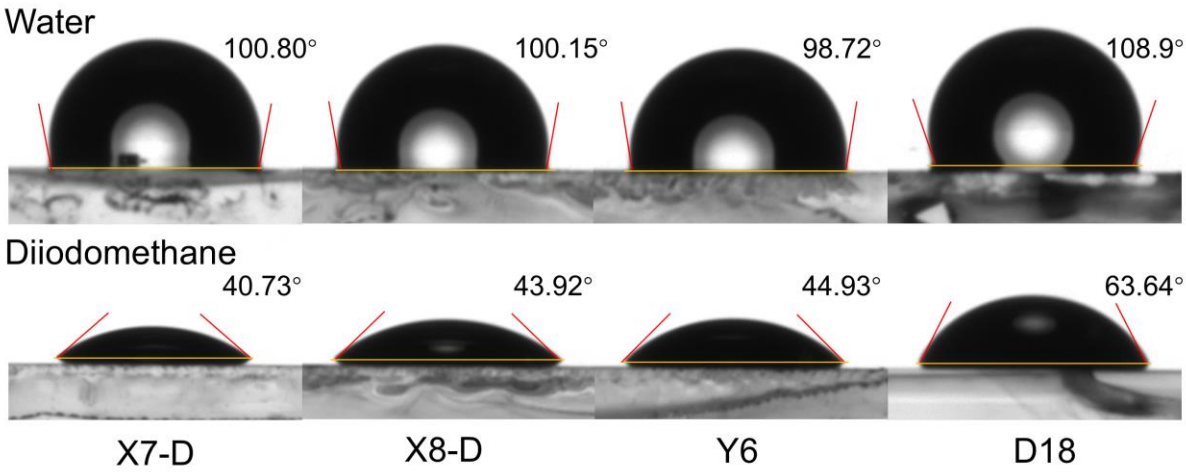

Fig. S18 Contact angle images of X7-D, X8-D, Y6, and D18.

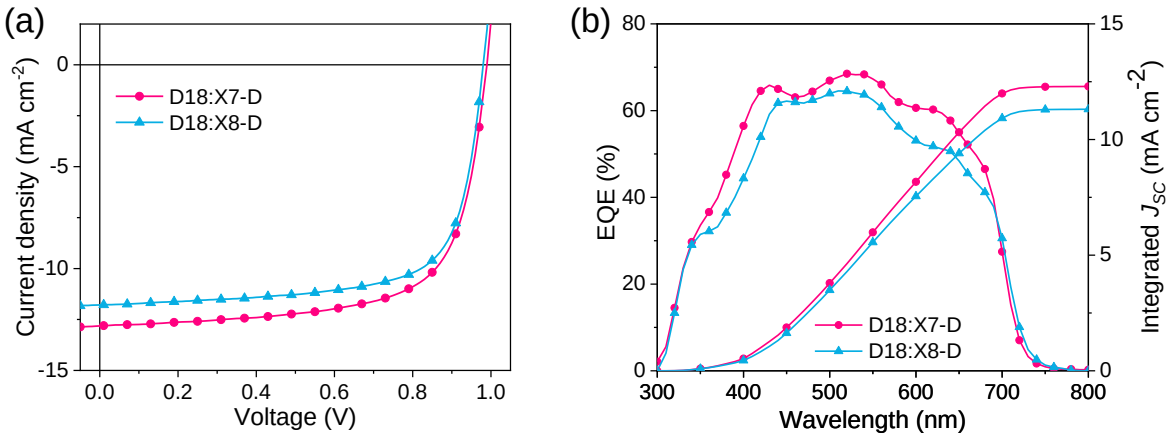

Fig. S19 (a) Optimized *J*–*V* curves and (b) EQE spectra and corresponding integrated current density of optimized binary devices based on D18:X7-D and D18:X8-D.

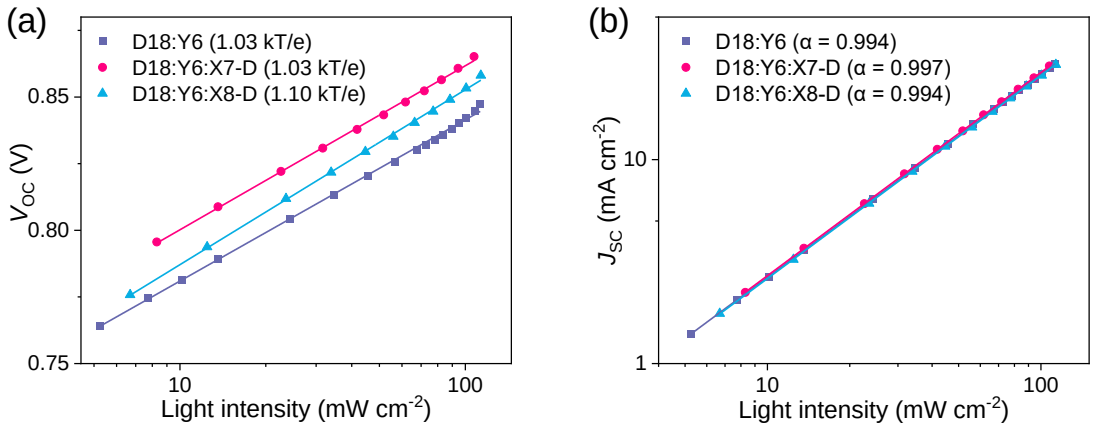

Fig. S20 (a) Dependence of V_{OC} on the P_{light} for devices. (b) Dependence of J_{SC} on the P_{light} for devices.

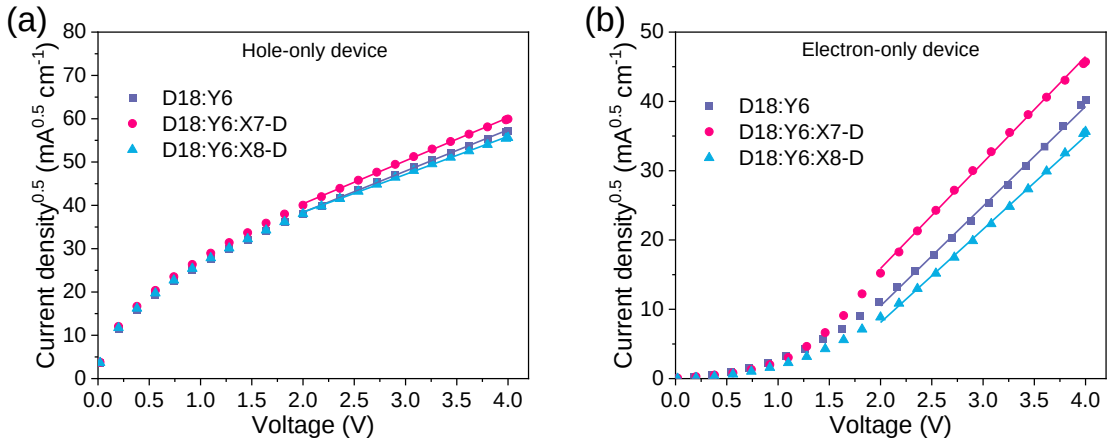

Fig. S21 $J^{0.5}$–*V* curves of (a) hole-only devices and (b) electron-only devices.

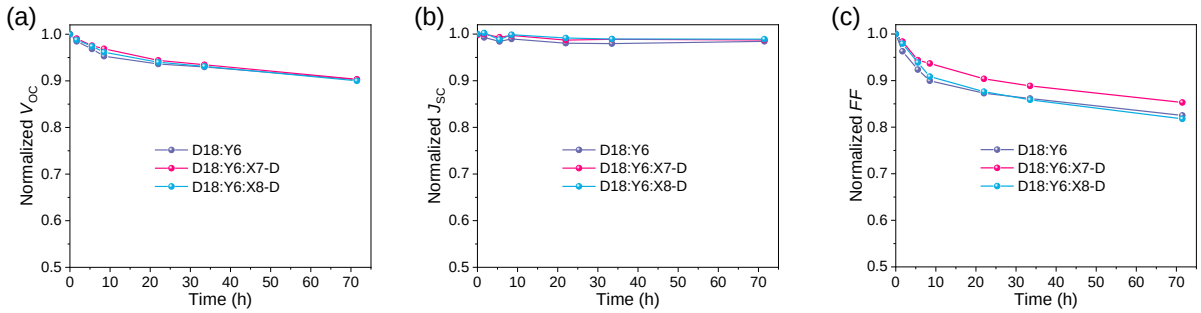

Fig. S22 The normalized values of (a) V_{OC}, (b) J_{SC}, and (c) FF versus aging time under constant heating at 80 °C.

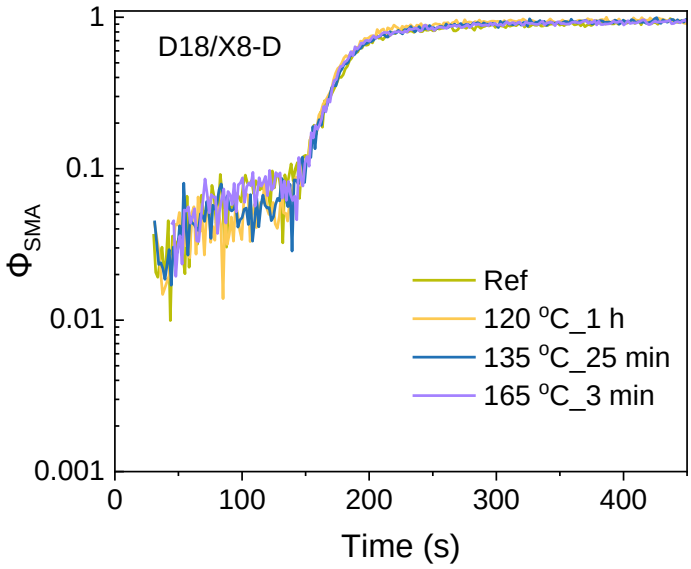

Fig. S23 SIMS diffusion profiles of reference and annealed D18/X8-D bilayer.

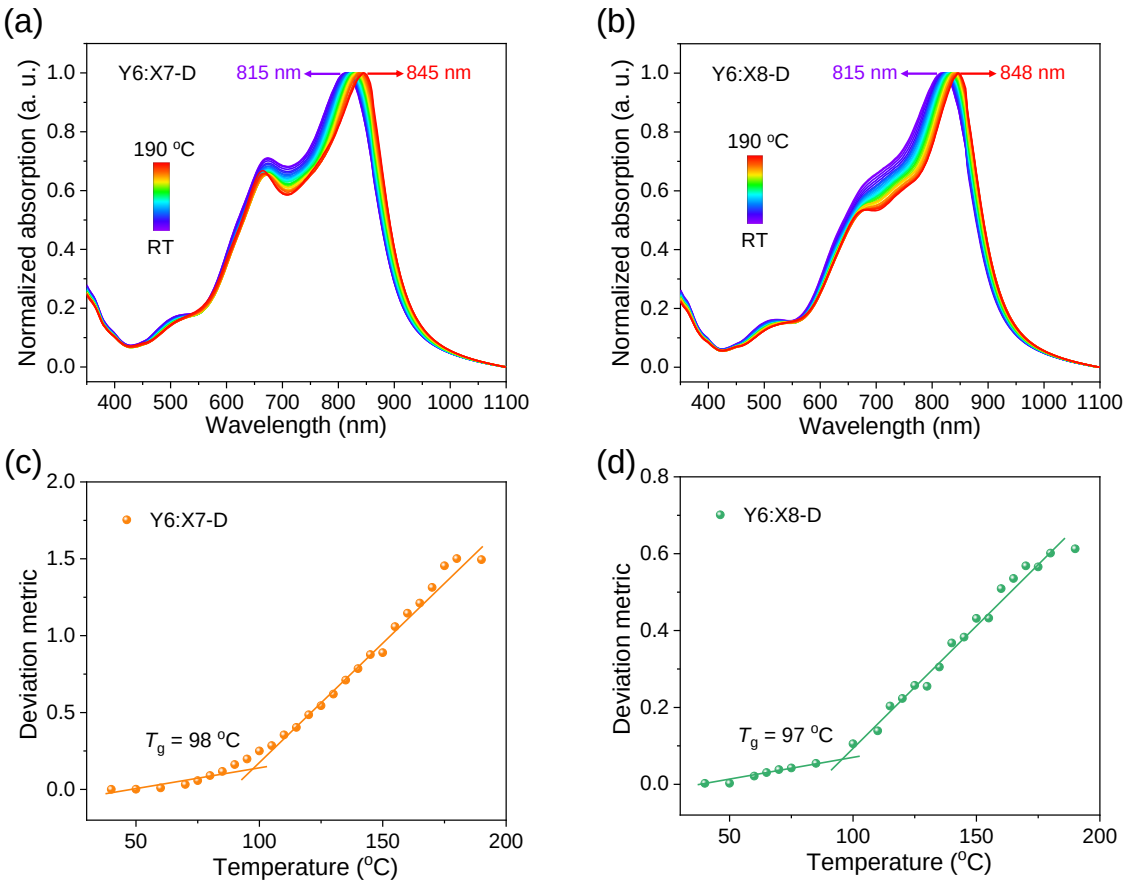

Fig. S24 (a-b) The temperature-dependent absorption spectra and (c-d) The temperature-dependent variations of absorption deviation of Y6:X7-D (7:1 *w*/*w*) and Y6:X8-D (7:1 *w*/*w*) blend films.

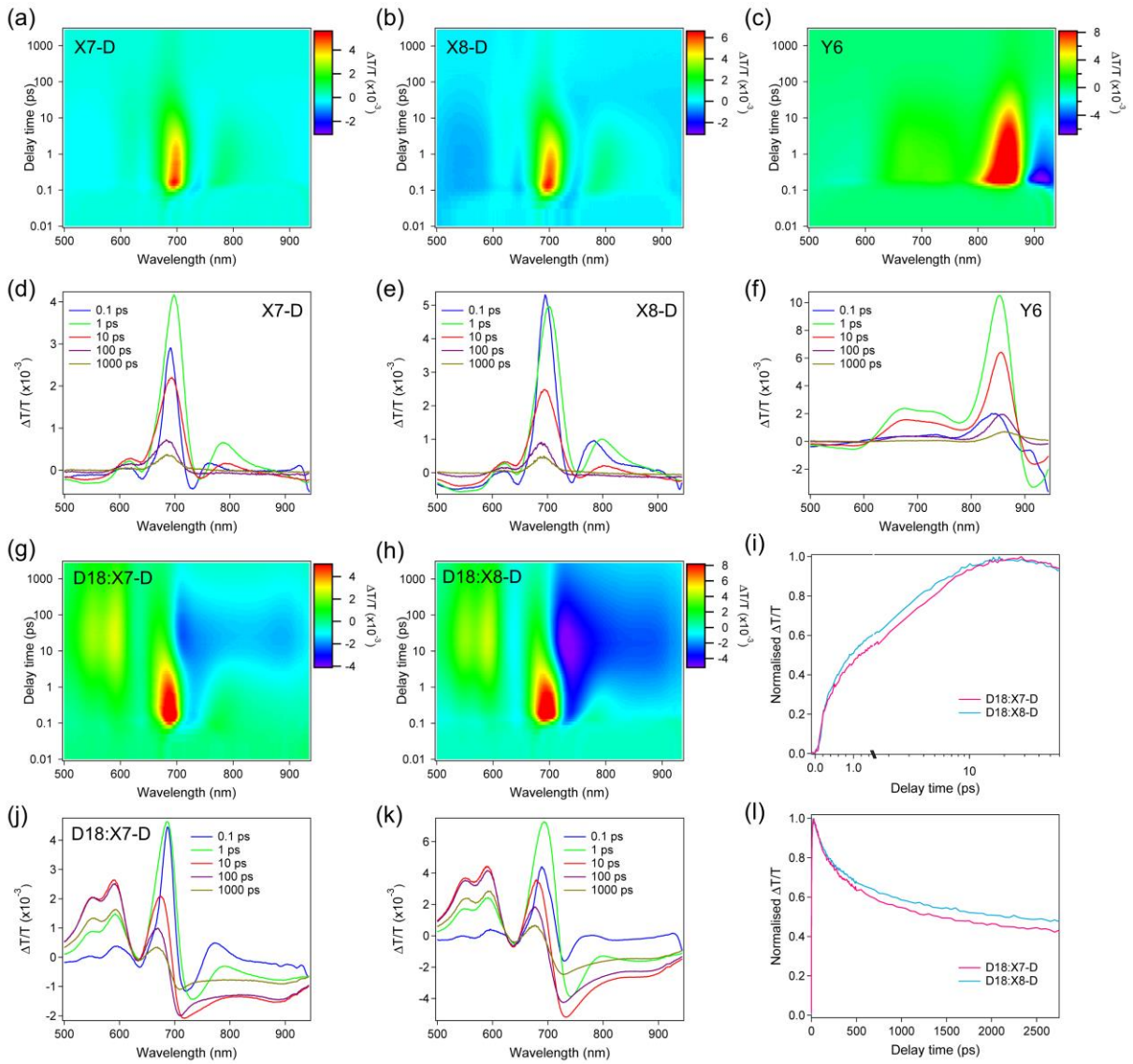

Fig. S25 TA images and corresponding TA spectra of (a, d) X7-D, (b, e) X8-D, and (c, f) Y6 pure films, as well as (g, j) D18:X7-D and (h, k) D18:X8-D blend films with various decay times. (i) Hole transfer kinetics of the GSB probed at 586 and 578 nm for D18:X7-D- and D18 blend films, respectively. (l) Charge carrier lifetime analysis in the blend films.

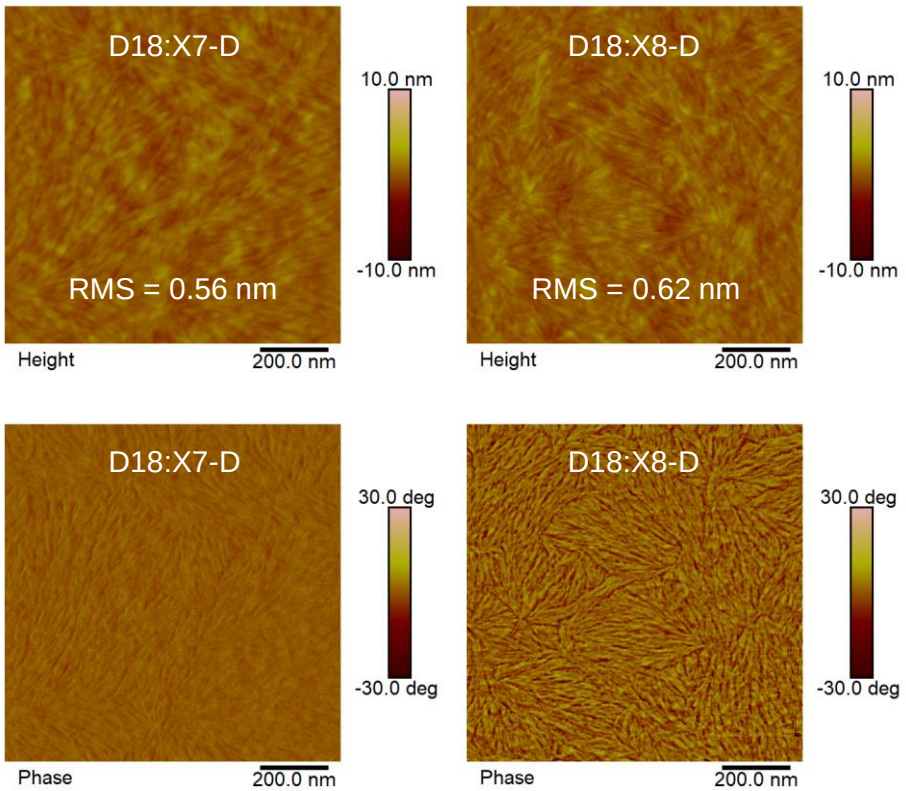

Fig. S26 AFM height and phase images for D18:X7-D and D18:X8-D binary films.

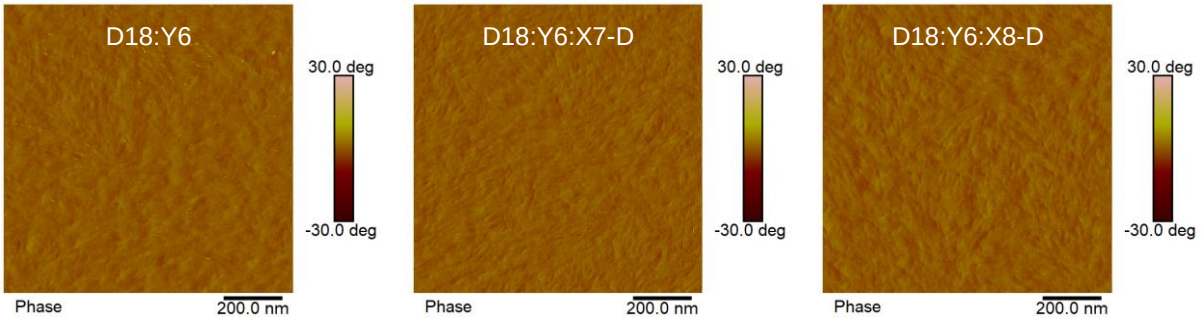

Fig. S27 AFM phase images of D18:Y6, D18:Y6:X7-D, and D18:Y6:X8-D blend films.

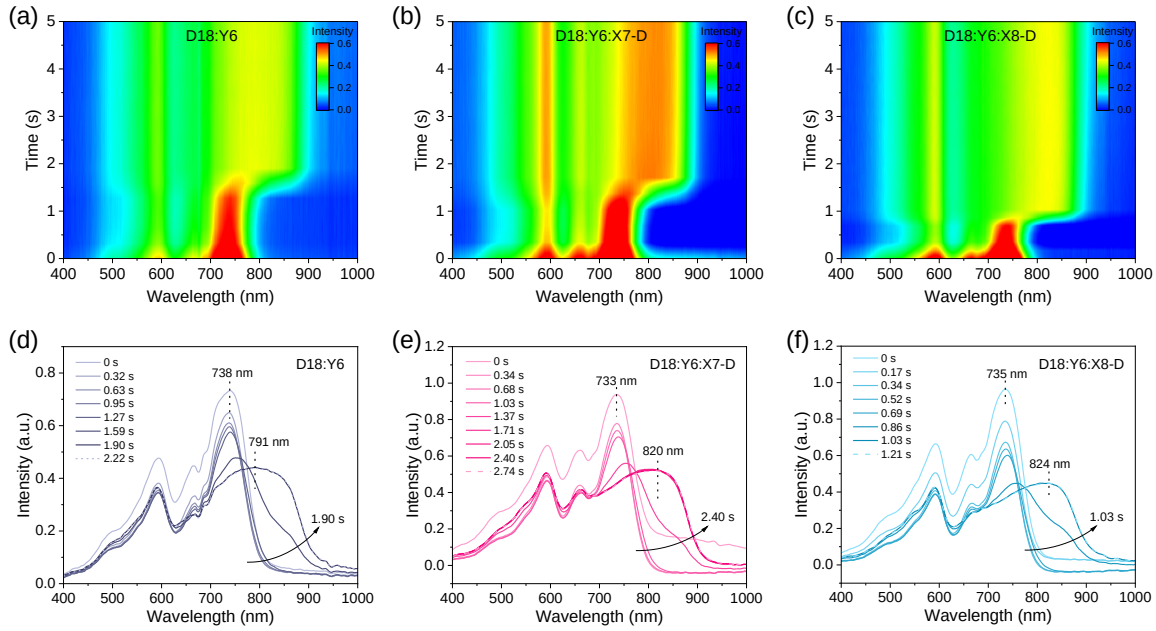

Fig. S28 (a-c) In-situ 2D UV−vis absorption profiles of three blend systems during spin coating. (d-f) In-situ UV−vis absorption line profiles of three blend systems during spin coating.

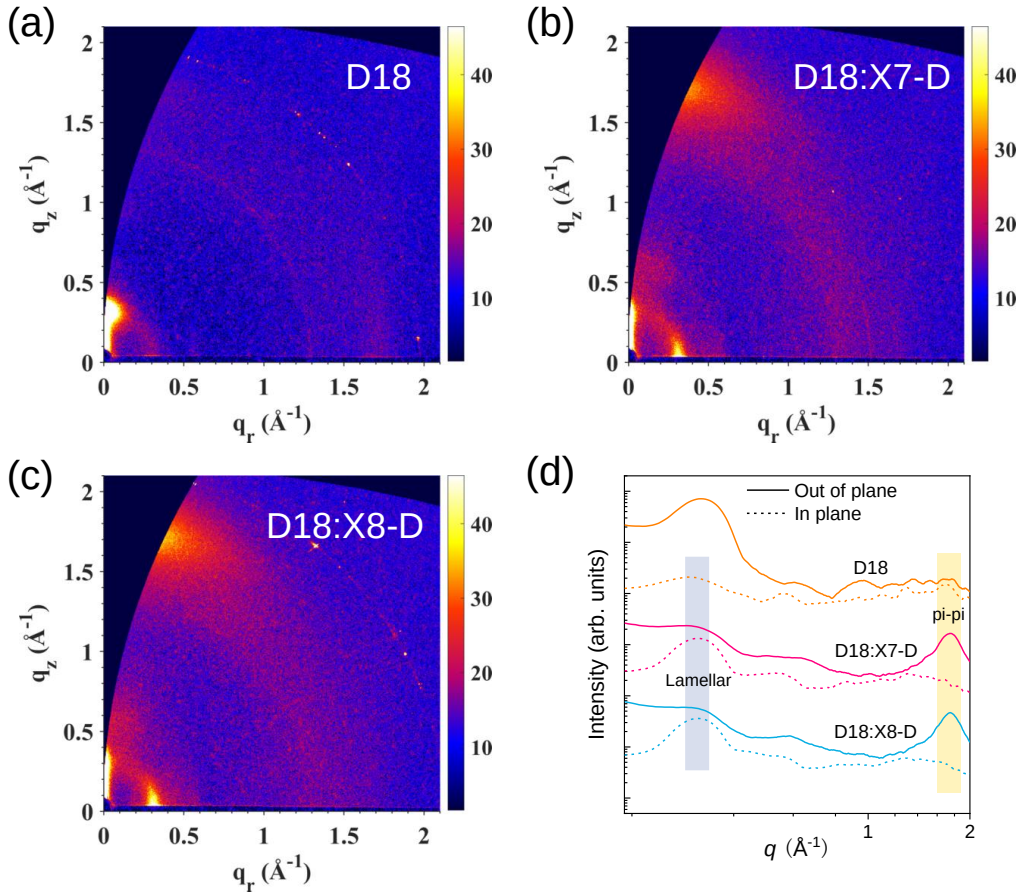

Fig. S29 (a-c) 2D GIWAXS patterns and (d) 1D scattering profiles of the D18, D18:X7-D, and D18:X8-D films.

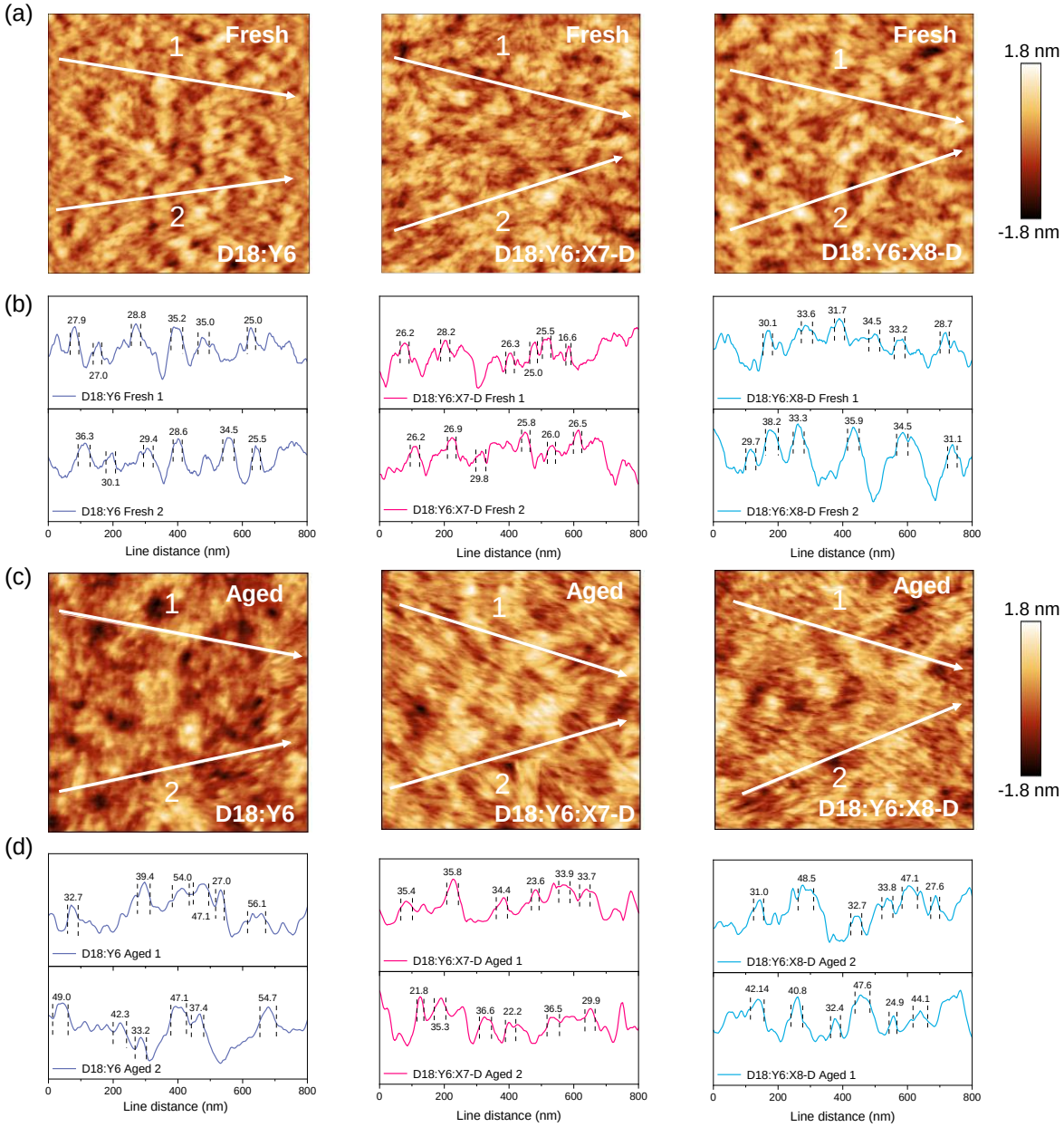

Fig. S30 (a, c) AFM height images (size: 1 μm × 1 μm) and (b, d) Line profiles across the AFM images of the fresh and aged binary and ternary blend films.

Supporting tables

Table S1. Optical and electrochemical properties of X7-D and X8-D.

Acceptor	λ_{max}^{sol} [nm]	λ_{max}^{film} [nm]	λ_{onset}^{film} [nm]	E_g^{opt} [eV]	HOMO [eV]	LUMO [eV]
X7-D	649	680	738	1.68	-5.84	-3.92
X8-D	658	687	748	1.66	-5.88	-3.92

Table S2. The contact angle with water and diiodomethane (DIM), the calculated surface energy, and Wetting coefficient for various films.

Film	θ_{water} (°)	θ_{DIM} (°)	$\gamma^{d\,a}$ (mN m^{-1})	$\gamma^{p\,b}$ (mN m^{-1})	γ^{c} (mN m^{-1})	$\chi^{D18-A\,d}$	$\chi^{Y6-A\,d}$	$\omega_{A_2}{}^{e}$
X7-D	100.80	40.73	39.02	0.0033	39.02	0.96	0.005	-1.076
X8-D	100.15	43.92	39.06	0.013	39.07	0.97	0.006	-1.081
Y6	98.72	44.93	38.01	0.086	38.10	0.82	--	
D18	108.9	63.64	27.73	0.0000099	27.73	--	--	

[a] Surface tension from dispersion component. [b] Surface tension from polarity component. [c] The total surface tension is calculated through the equation of $\gamma = \gamma^p + \gamma^d$. [d] The Flory-Huggins interaction parameter between A and B is calculated with the equation of $\chi^{A-B} = k\,(\sqrt{\gamma_A} - \sqrt{\gamma_B})^2$.

[e] The wetting coefficient (ω) of the third component A_2 in the mixture of D:A_1 can be expressed according to Young's equation of

$$\omega_{A_2} = \frac{\gamma_{A_1/A_2} - \gamma_{D/A_2}}{\gamma_{D/A_1}}$$

The interfacial tension between A and B can be calculated through the Wu's Equation of

$$\gamma_{A/B} = \gamma_A + \gamma_B - 4\left(\frac{\gamma_A{}^d \gamma_B{}^d}{\gamma_A{}^d + \gamma_B{}^d} + \frac{\gamma_A{}^p \gamma_B{}^p}{\gamma_A{}^p + \gamma_B{}^p}\right)$$

Table S3. Recent reports regarding the binary and ternary devices based on D18:Y6.

Active layer	V_{OC} (V)	J_{SC} (mA cm^{-2})	FF	PCE (%)	Reference
D18:Y6:X7-D	0.871	27.60	0.784	18.80	This work
D18:Y6:BTR	0.850	27.82	0.792	18.75	4
D18:Y6:IDTT-SiO-IC	0.896	26.72	0.784	18.77	5
D18:Y6:BTP-H2-γ	0.871	27.12	0.784	18.51	6
D18:Y6:ZW1	0.860	27.97	0.769	18.50	7
D18:Y6:SN-O	0.876	26.80	0.781	18.30	8
D18:Y6:L8-CBIC-Cl	0.870	27.05	0.761	18.04	9
D18:Y6:MAZ-2	0.860	27.62	0.754	17.91	10
D18:Y6:$PC_{61}BM$	0.870	26.48	0.776	17.89	11
D18:Y6:BTPR	0.863	27.65	0.746	17.80	12
D18:Y6:BTIC-γ-2CN	0.882	25.27	0.791	17.61	13
D18:Y6:BTR-Cl	0.858	26.90	0.744	17.20	14
D18:Y6:PM6	0.852	25.55	0.728	15.85	15
D18:Y6:$NC_{70}BA$	0.860	24.67	0.705	14.96	16
D18:Y6	0.870	27.10	0.779	18.30	17
D18:Y6	0.848	27.11	0.789	18.14	18
D18:Y6	0.853	26.82	0.765	17.50	19
D18:Y6	0.859	27.70	0.766	18.22	20
D18:Y6	0.870	26.04	0.782	17.82	21

Table S4. Photovoltaic performances of binary and ternary OSCs based on D18:X7-D, D18:X8-D, D18:Y6, D18:Y6:X7-D and D18:Y6:X8-D photoactive layers with different weight ratios.

Active layer	V_{OC} (V)	J_{SC} (mA cm^{-2})	FF	PCE (%)
D18:X7-D (1:1.4)	0.990	12.82	68.93	8.74
D18:X8-D (1:1.4)	0.980	11.79	71.15	8.21
D18:Y6 (1:1.6)	0.859	25.90	78.25	17.40
D18:Y6:X7-D (1:1.5:0.1)	0.863	26.10	79.26	17.81
D18:Y6:X7-D (1:1.4:0.2)	0.871	27.60	78.44	18.80
D18:Y6: X7-D (1:1.2:0.4)	0.892	24.05	75.45	16.15
D18:Y6:X8-D (1:1.5:0.1)	0.861	26.01	77.70	17.39
D18:Y6:X8-D (1:1.4:0.2)	0.873	24.98	75.07	16.39
D18:Y6:X8-D (1:1.2:0.4)	0.882	24.12	74.17	15.80

Table S5. The hole and electron mobilities of different devices.

Active layer	μ_h ($\times10^{-4}$ cm^2 V^{-1} s^{-1})	μ_e ($\times10^{-4}$ cm^2 V^{-1} s^{-1})	μ_e/μ_h
D18:Y6	2.69	7.16	2.66
D18:Y6:X7-D	3.20	7.74	2.42
D18:Y6:X8-D	2.12	6.09	2.87

Table S6. Diffusion coefficients for different systems at various temperatures

System	Annealing T (°C)	Time (min)	D (cm^2/s)	D_{85} (cm^2/s)
D18/Y6	120	60	4.3×10^{-15}	3.0×10^{-16}
	135	25	2.0×10^{-14}	
	165	3	8.9×10^{-14}	
D18/Y6:X7-D	120	60	3.7×10^{-15}	1.7×10^{-16}
	135	25	1.2×10^{-14}	
	165	3	9.1×10^{-14}	

D18/Y6:X8-D	135	25	1.4×10^{-14}	1.8×10^{-16}
	165	3	1.2×10^{-13}	

Table S7. Summary of the detailed fitting parameters of different blends.

Active layer	A_1	τ_1 (ps)	A_2	τ_2 (ps)
D18:X7-D	0.312	0.3020±0.0119	0.688	3.7116±0.0748
D18:X8-D	0.419	0.3677±0.0128	0.581	3.2677±0.0935
D18:Y6	0.296	0.9868±0.0534	0.704	29.789±0.917
D18:Y6:X7-D	0.302	0.2349±0.0133	0.698	13.794±0.253
D18:Y6:X8-D	0.259	0.4160±0.0258	0.741	15.299±0.295

Table S8. Summary of the detailed data of GIWAXS Characterization.

	Out of plane (010)				In plane (100)			
	q (Å^{-1})	*d* (Å)	*FWHM* (Å^{-1})	*CCL* (Å)	*q* (Å^{-1})	*d* (Å)	*FWHM* (Å^{-1})	*CCL* (Å)
Y6	1.780	3.53	0.275	18.28	0.295	21.30	0.125	40.21
X7-D	1.730	3.63	0.370	13.59	0.475	13.23	0.165	30.46
X8-D	1.725	3.64	0.319	15.76	0.420	14.96	0.165	30.46
D18:Y6	1.770	3.55	0.256	19.64	0.305	20.60	0.109	46.12
D18:X7-D	1.750	3.59	0.271	18.55	0.315	20.01	0.095	52.91
D18:X8-D	1.750	3.59	0.249	20.19	0.315	20.01	0.094	53.47
D18:Y6:X7-D	1.780	3.53	0.252	19.95	0.305	20.60	0.114	44.09
D18:Y6:X8-D	1.780	3.53	0.249	20.19	0.305	20.60	0.113	44.48

Supporting References

1 Y. Shen, A. R. Hosseini, M. H. Wong and G. G. Malliaras, *ChemPhysChem*, 2004, **5**, 16-25.

2 M. Ghasemi, N. Balar, Z. Peng, H. Hu, Y. Qin, T. Kim, J. J. Rech, M. Bidwell, W. Mask, I. McCulloch, W. You, A. Amassian, C. Risko, B. T. O'Connor and H. Ade, *Nat. Mater.*, 2021, **20**, 525-532.

3 H. Fu, J. Yao, M. Zhang, L. Xue, Q. Zhou, S. Li, M. Lei, L. Meng, Z. G. Zhang and Y. Li, *Nat. Commun.*, 2022, **13**, 3687.

4 X. Kong, L. Zhan, Z. Li, Y. Yang, Y. Liu, H. Qiu, X. Sun, H. Hu, R. Sun, J. Min, S. Yin, W. Fu and H. Chen, *Aggregate*, 2024, e553.

5 F. Meng, Y. Qin, Y. Zheng, Z. Zhao, Y. Sun, Y. Yang, K. Gao and D. Zhao, *Angew. Chem. Int. Ed.*, 2023, **62**, e202217173.

6 Y. Zhu, X. Shen, H. Lai, M. Pu, Y. Zhu, X. Lai, S. Xiong and F. He, *Nano Energy*, 2023, **118**, 108991.

7 W. Zou, C. Han, X. Zhang, J. Qiao, J. Yu, H. Xu, H. Gao, Y. Sun, Y. Kan, X. Hao, G. Lu, Y. Yang and K. Gao, *Adv. Energy Mater.*, 2023, **13**, 2300784.

8 R. Xu, Y. Jiang, F. Liu, W. Su, W. Liu, S. Xu, H. Fan, C. Jiang, Q. Zong, W. Zhang and X. Zhu, *Chem. Eng. J.*, 2023, **464**, 142507.

9 C. Zhang, R. Zheng, H. Huang, G. Ran, W. Liu, Q. Chen, B. Wu, H. Wang, Z. Luo, W. Zhang, W. Ma, Z. Bo and C. Yang, *Adv. Energy Mater.*, 2024, **14**, 2303756.

10 X. Gao, X. Ma, Z. Liu, J. Gao, Q. Qi, Y. Yu, Y. Gao, Z. Ma, L. Ye, J. Min, J. Wen, J. Gao, F. Zhang and Z. Liu, *ACS Appl. Mater. Interfaces*, 2022, **14**, 23701-23708.

11 J. Qin, L. Zhang, Z. Xiao, S. Chen, K. Sun, Z. Zang, C. Yi, Y. Yuan, Z. Jin, F. Hao, Y. Cheng, Q. Bao and L. Ding, *Sci. Bull.*, 2020, **65**, 1979-1982.

12 Y. Zhang, G. Cai, Y. Li, Z. Zhang, T. Li, X. Zuo, X. L and Y. Lin, *Adv. Mater.*, 2021, **33**, 2008134.

13 C. Sun, X. Lai, T. Rehman, H. Lai, C. Ke, X. Shen, Y. Zhu, L. Tian and F. He, *J. Mater. Chem. C*, 2022, **10**, 17174-17181.

14 H. Zhao, B. Lin, J. Xue, H. B. Naveed, C. Zhao, X. Zhou, K. Zhou, H. Wu, Y. Cai, D. Yun,

Z. Tang and W. Ma, *Adv. Mater.*, 2022, **34**, 2105114.

15 Z. Liu, *Org. Electron.*, 2021, **93**, 106153.

16 Z. Liu and H. Wang, *Nanotechnology*, 2021, **33**, 065206.

17 J. Wang, Y. Wang, P. Bi, Z. Chen, J. Qiao, J. Li, W. Wang, Z. Zheng, S. Zhang, X. Hao and J. Hou, *Adv. Mater.*, 2023, **35**, 2301583.

18 K. Wang, F. Zhao, Y. Zhu, Y. He, Z. Liu, X. Han, Q. Ai, X. Shen, B. Li, J. Zhang, Y. Lin, C. Wang and D. He, *J. Mater. Chem. A*, 2024, **12**, 12208-12215.

19 H. Bai, Q. An, H. Zhi, M. Jiang, A. Mahmood, L. Yan, M. Liu, Y. Liu, Y. Wang and J. Wang, *ACS Energy Lett.*, 2022, **7**, 3045-3057.

20 Q. Liu, Y. Jiang, K. Jin, J. Qin, J. Xu, W. Li, J. Xiong, J. Liu, Z. Xiao, K. Sun, S. Yang, X. Zhang and L. Ding, *Sci. Bull.*, 2020, **65**, 272-275.

21 R. Yang, J. Tian, W. Liu, Y. Wang, Z. Chen, T. P. Russell and Y. Liu, *Chem. Mater.*, 2022, **34**, 7293-7391.